5 RESEARCH ACTIVITIES

5.1 NUCLEAR PHYSICS

N. Madhavan

The first stage of National Array of Neutron Detectors (NAND), consisting of 50 liquid scintillators of 5" x 5" size, was successfully tested with beam using indigenously built electronics and VME-based data acquisition system by adapting LAMPS software. Neutrons and gamma rays could be resolved in all the detectors thereby facilitating neutron multiplicity generation. The specially designed beam-dump was found to work very well. Subsequently, the remaining 50 detectors have also been assembled in the mounting structure and first experiment will be taken up soon.

Lifetime measurements have been carried out in Gamma Detector Array (GDA) beam-line after the revival of Plunger setup. Coulomb excitation studies and g-factor measurements were extended to few more nuclei. The clover germanium detectors of IUAC have arrived from TIFR after the successful INGA campaign. Other institute detectors are awaited to proceed with HYRA-INGA combined facility. An earlier INGA experiment at IUAC resulted in the identification of twin chiral bands in 102Rh (Tonev et al.) which was reported in PRL this year.

Heavy Ion Reaction Analyzer (HIRA) was used to study fusion cross-section around the barrier and to measure evaporation residue transmission efficiency for $^{16}O + ^{64}Zn$ and $^{32}S + ^{48}Ti$ systems. The TIFR spin spectrometer and HIGRASP setup were used in HYRA beam-line for the study of Giant Dipole Resonance (GDR) built on excited states.

The superconducting doublet for HYbrid Recoil mass Analyzer (HYRA) was energized up to a current of 75 A. With 100 A current, 2 T field is expected at 10 cm radius near the pole positions. The electrode assembly of the electrostatic dipole (ED) has been set up and aligned in a clean cabin and subsequently placed in the ED chamber. Quadrupole doublet Q6-Q7 have been aligned which will provide the entrance direction to ED.

The General Purpose Scattering Chamber (GPSC) has been used for several scattering, breakup/transfer, fission and incomplete fusion reactions. A new addition this year was the setting up of 16 CsI detectors for light charged particle detection which worked well.

International conference FUSION14, sixth in the series, was held at IUAC from February 24 to 28, 2014. A total of 30 researchers representing groups outside India and close to 100 Indian participants including students attended the conference. A two-day school was held prior to the conference on February 21 and 22 for the benefit of students and young researchers in the topics of the conference. Workshops on ancillary detectors for nuclear physics facilities, on the production and use of RIBs using HYRA and on the Theory of Nuclear Spectroscopy were held at IUAC during the course of the year.

5.1.1 Evaporation residue cross-section measurements for $^{16}O + ^{64}Zn$ and $^{32}S + ^{48}Ti$ reactions

Maninder Kaur[1], B.R. Behera[1], Gulzar Singh[1], Varinderjit Singh[2], S. Nath[3], N. Madhavan[3], G. Mohanto[3], I. Mukul[3], Davinder Siwal[3,4], Meenu Thakur[1], Kushal Kapoor[1], Priya Sharma[1], Tathagata Banerjee[3], A. Jhingan[3], Indu Bala[3], S. Muralithar[3], T. Varughese[3], A. Saxena[5], B.K. Nayak[5] and M.B. Chatterjee[3]

[1]Department of Physics, Panjab University, Chandigarh 160014, India
[2]Department of Physics, National Institute of Technology, Jalandhar 144001, India
[3]Inter University Accelerator Centre, Aruna Asaf Ali Marg, New Delhi 110067, India
[4]Department of Physics and Astrophysics, University of Delhi, Delhi 110007, India
[5]Nuclear Physics Division, Bhabha Atomic Research Centre, Mumbai 400085, India

Evaporation residue (ER) cross-sections for the formation of the compound nucleus (CN) ^{80}Sr*, populated through mass symmetric ^{32}S+^{48}Ti and mass asymmetric channel ^{16}O+^{64}Zn, have been measured in the excitation energy range of 52.8 - 73.1 MeV. The measurements have been performed using HIRA [1] facility at IUAC, New Delhi. The ERs were separated from the other contamination and were detected at the focal plane using an MWPC [2]. Two silicon surface barrier detectors were placed inside the target chamber at angles of 25° with respect to beam direction, for normalization purposes. The transmission efficiency of HIRA was measured using an HPGe detector mounted at the target chamber. The characteristic γ-rays from the ERs were detected in singles as well as in coincidence with the ERs for both the systems at E* = 57 MeV. The ratio of the counts in a characteristic γ-peak in the gated spectrum to that in the singles spectrum gives the transmission efficiency of HIRA (η_{HIRA}) for that particular ER. Figure 1 shows the ER-gated and the singles characteristic γ-ray spectra for both the systems.

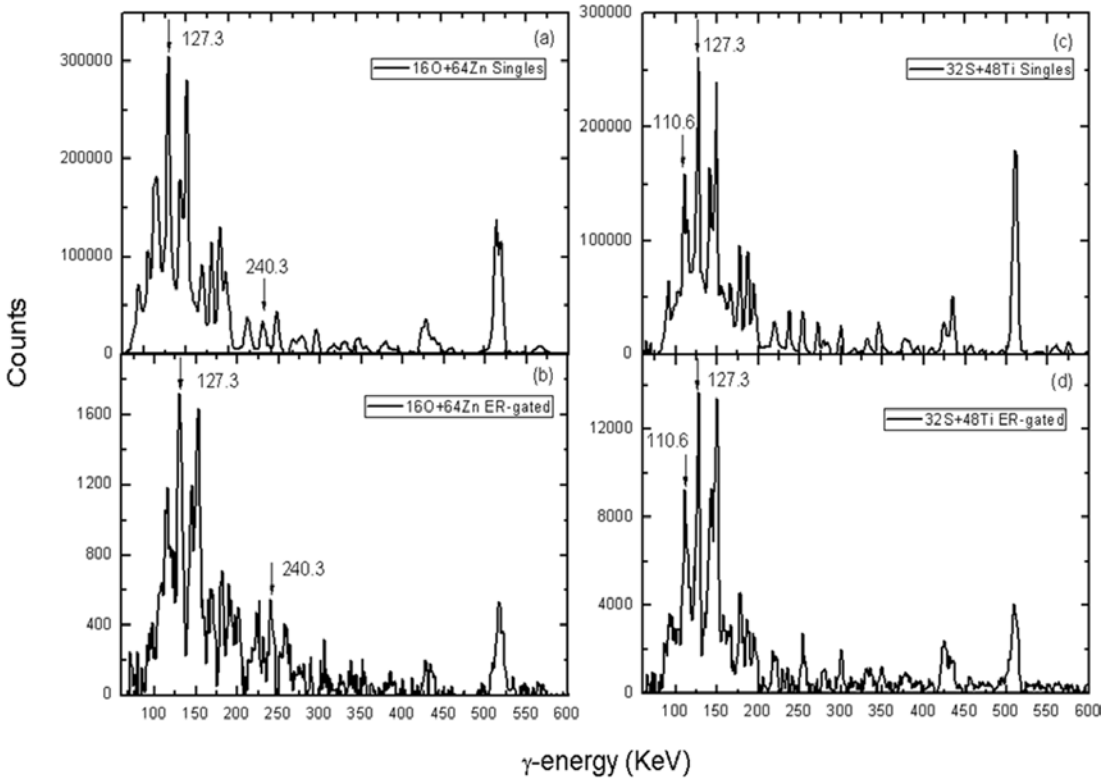

Fig. 1: Characteristic γ-spectra from ERs: (a) γ in singles for the system ^{16}O+^{64}Zn and (b) γ in coincidence with ERs for the system ^{16}O+^{64}Zn, (c) γ in singles for the system ^{32}S+^{48}Ti and (d) γ in coincidence with ERs for the system ^{32}S+^{48}Ti.

Further, η_{HIRA} for these systems was simulated using the Monte Carlo simulation code [3]. The efficiency values thus obtained are in reasonable agreement with experimentally obtained values. Table I shows measured as well as simulated η_{HIRA} for some of the populated ERs.

TABLE I : Transmission efficiency of ERs through HIRA at E* = 57 MeV.

System	ER	Experimental η_{HIRA}	η_{HIRA} from TERS
^{32}S+^{48}Ti	^{77}Kr (2pn)	4.9%	5.1%
^{32}S+^{48}Ti	^{76}Br (3pn)	6.5%	5.5%
^{16}O+^{64}Zn	^{77}Kr (2pn)	0.7%	0.8%
^{16}O+^{64}Zn	^{76}BR (3pn)	0.9%	0.8%

TERS was further used to obtain η_{HIRA} for the ER channels which could not be obtained experimentally. The average ER transmission efficiency for all the ERs through the HIRA was obtained by taking the weighted average of the efficiency for different evaporation channels at each energy (Elab). Relative abundance of different exit channels was estimated using PACE. Table II shows the average η_{HIRA} for both the systems.

TABLE II: Average value of η_{HIRA} and corresponding cross-sections at different energies.

System	Elab (MeV)	E* (MeV)	η_{HIRA}	σ_{ER}
$^{16}O+^{64}Zn$	66.6	52.8	0.47%	835.7 ± 187.9
$^{16}O+^{64}Zn$	71.8	57.0	0.42%	963.2 ± 144.5
$^{16}O+^{64}Zn$	77.8	61.8	0.33%	1126.4 ± 168.9
$^{16}O+^{64}Zn$	82.1	65.2	0.23%	1476.2 ± 221.4
$^{16}O+^{64}Zn$	89.1	70.8	0.23%	1350.0 ± 203
$^{16}O+^{64}Zn$	91.9	73.1	0.23%	1392.9 ± 208.9
$^{32}S+^{48}Ti$	95.0	52.8	4.02 %	237.0 ± 35.6
$^{32}S+^{48}Ti$	102.0	57.0	3.05%	367.0 ± 53.6
$^{32}S+^{48}Ti$	110.0	61.8	1.40%	1036.0 ± 155.4
$^{32}S+^{48}Ti$	117.0	66.0	1.70%	691.0 ± 104
$^{32}S+^{48}Ti$	125.0	70.8	1.72%	370.8 ± 55.6

Using average η_{HIRA}, ER cross-sections (σ_{ER}) were obtained using the expression

$$\sigma_{ER} = \frac{Y_{ER}}{Y_{norm}} \left(\frac{\partial \sigma}{\partial \Omega} \right)_{Ruth} \Omega_{mon} \frac{1}{\eta_{HIRA}},$$

where YER is the ER yield at the focal plane of HIRA, Y_{norm} is the elastically scattered events detected by the monitor detector, $(d\sigma/d\Omega)_{Ruth}$ is the Rutherford scattering differential cross-section, Ω_{mon} is the solid angle subtended by the monitor detector. The preliminary cross-sections for both the systems are tabulated in Table II. Theoretical calculation is in progress. The aim of the present work is to fit cross-sections with CCFULL [4] results and generate the corresponding spin distribution. This spin distribution will be used to explain deviations appearing in the light particles evaporation spectra for the symmetric systems as reported in [5].

References

[1] A.K. Sinha et al., Nucl. Instrum. Methods A 596, 248 (2008).
[2] A. Jhingan et al., DAE Symp. Nucl. Phys. 52 B, 585 (2007).
[3] S. Nath, Comput. Phys. Commun. 180, 2392 (2009).
[4] K. Hagino, N. Rowley and A.T. Kruppa, Comput. Phys. Commun. 123, 143 (1999).
[5] J. Kaur et al., Phy. Rev. C 70, 017601 (2004).

5.1.2 Spin gated giant dipole resonance widths in ^{144}Sm

Ish Mukul[1], A. Roy[1], P. Sugathan[1], G. Mohanto[1], J. Gehlot[1], N. Madhavan[1], S. Nath[1], R. Dubey[1], T. Banerjee[1], N. Saneesh[1], I. Mazumdar[2], D.A. Gothe[2], M. Kaur[3], A.K. Rhine Kumar[4] and P. Arumugam[4]

[1]Nuclear Physics Group, Inter University Accelerator Centre, New Delhi 110067, India

[2]Department of Nuclear and Atomic Physics, Tata Institute of Fundamental Research, Mumbai 400005, India
[3]Department of Physics, Panjab University, Chandigarh 160014, India
[4]Department of Physics, Indian Institute of Technology Roorkee, Roorkee 247667, Uttarakhand, India

Study of collective modes of excitations in many-body systems has been an active field of research for a long time. Atomic nuclei provide an excellent laboratory for studying such modes as they display a much richer spectrum of collective modes than other quantum systems. The phenomenon of giant dipole resonance (GDR), built on excited states, is one such collective mode in which all nucleons participate [1]. It is one of the few known tools to study nuclear properties at high extremes. GDR properties, namely, energy centroid and resonance width could be related to nuclear deformation and damping mechanism. The resonance widths are also related to nuclear shear viscosity [2]. In heavy ion-induced reaction, populated at a fixed excitation energy, the increase in GDR width is due to the coupled effect of *T* and *J*. It is an experimental challenge to decouple these effects. In recent years, several experiments have been carried out to study the dependence of temperature and angular momentum on GDR observables like centroid, width and strength. We have measured high-energy γ-rays from de-excitation of hot and rotating ^{144}Sm using ^{28}Si+^{116}Cd reaction [3,4]. Data were analyzed using the statistical model code CASCADE [5] with necessary modifications for GDR. With the help of a 4π spin spectrometer [6], we have measured fold gated GDR γ-spectrum. We also deduced GDR widths as a function of angular momentum and temperature at a given excitation energy (Figure 2). The measurements have been performed in the temperature range of 1-2 MeV where shell effects wash out and the nucleus behaves as a hot rotating liquid drop. Thermal shape fluctuations play important part in the increase of resonance width in this T range. TSFM calculations [7] have been performed for this system. GDR widths are consistent with this model. Also, Kusnezov parameterization [8] holds good for this nucleus over the entire experimental range.

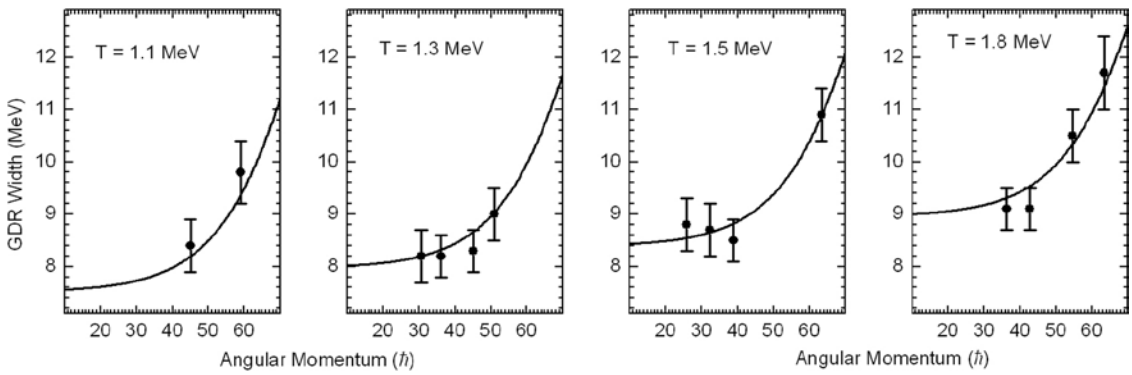

Fig.2: GDR widths as a function of angular momentum. Solid lines are calculations by Kusnezov's parameterization [8].

References

[1] K.A. Snover, Ann. Rev. Nucl. Part. Sci. 36, 545 (1985); J.J. Gaardhoje, Ann. Rev. Nucl. Part. Sci. 42, 483 (1992).
[2] N. D. Dang. Phys. Rev. C. 84, 034309 (2011).
[3] Ish Mukul *et al.,* Phys. Rev. C. 88, 024312 (2013).
[4] Ish Mukul *et al.,* EPJ Web of Conference 63, 01020 (2013).
[5] F. Puhlhofer, Nucl. Phys. A 280, 267 (1977).
[6] G. A. Kumar *et al.,* Nucl. Instr. Meth. A 611, 76 (2009).
[7] P. Arumugam *et al.,* Phys. Rev. C 69, 054313 (2004).
[8] D. Kusnezov *et al.,* Phys. Rev. Lett. 81, 542 (1998).

5.1.3 Study of fusion-fission dynamics in ^{19}F induced reactions

R. Dubey[1], G. Mohanto[1], T. Banerjee[1], N. Saneesh[1], D. Siwal1, A. Jhingan[1], P. Sugathan[1], G. Kaur[2], M. Thakur[2], R. Mahajan[2] and N. Joshi[3]

[1]Nuclear Physics Group, Inter University Accelerator Centre, New Delhi 110067, India
[2]Department of Physics, Panjab University, Chandigarh 160014, India
[3]Department of Physics and Astrophysics, Delhi University, Delhi 110007, India

Study of fission dynamics is an important topic of research in many heavy ion accelerator facilities. There are many reaction processes such as fusion fission, fast fission, quasi fission etc. which play important roles in the dynamics. Understanding and identifying the significance of each process is still a major challenge. In case of pre-equilibrium fission process, enhancement of mass width and larger angular anisotropy have been reported in recent works [1]. In addition, role of deformation of the reaction partners play important role in these processes. In order to study the role of entrance channel on fission fragment mass distribution, we have performed experiments with the ^{19}F+^{206,208}Pb systems and compared the results with ^{16}O+^{208}Pb system.

The experiments have been performed in the GPSC facility using Pelletron beams. Targets of ^{206,208}Pb with thicknesses of ~130 μg/cm^2 on carbon backings were fabricated at IUAC target laboratory. The enrichment of the target material was more than 96.3%. We have used pulsed beam of ^{19}F at laboratory energies ranging from 80 to 112 MeV forming compound nucleus (CN) ^{225,227}Pa* at different excitation energies. For extracting mass distribution, two MWPCs (8"x4") were placed at folding angles. Forward and backward detectors were placed at 35 cm and 27 cm, respectively, from the target. Two monitor detectors were placed at ±13° with respect to the beam direction to monitor beam flux. From the MWPC position signals, mass angle correlation and mass distribution of fission fragments were extracted which are shown in figure 3. No mass-angle correlation has been observed in this system. Further analysis of the data is in progress.

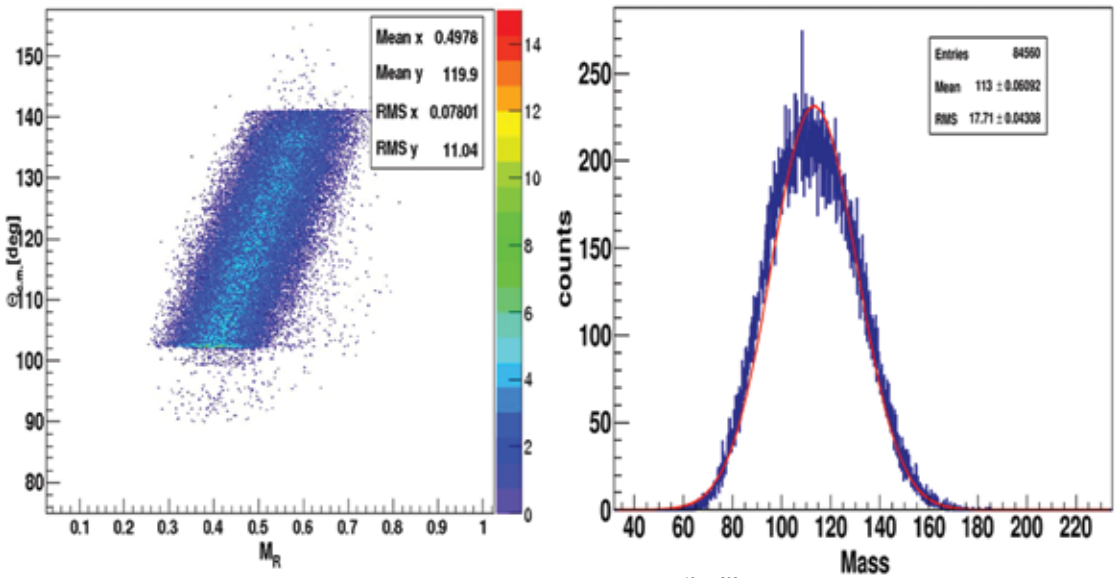

Fig. 3: Mass angle correlation and mass distribution for ^{19}F+^{208}Pb at E_{lab} = 112 MeV.

References

[1] D.J. Hinde et al, Physical Review C 53, 1290 (1996).

5.1.4 Fission fragment mass distributions for $^{16}O + ^{184}W$

Gayatri Mohanto[1], P. Sugathan[1], A. Jhingan[1], N. Saneesh[1], Rakesh Dubey[1], Tathagata Banerjee[1], Ish Mukul[1], Maninder Kaur[2] and Meenu Thakur[2]

[1]Inter University Accelerator Centre, Aruna Asaf Ali Marg, New Delhi 110067, India
[2]Department of Physics, Panjab University, Chandigarh 160014, India

Formation of heavy nuclei is one of the major goals in present day experimental nuclear physics. The competition of fission with fusion hinders the heavy nuclei formation and hence study of the fission dynamics has become important. In case of nuclear fusion, fission can take place before or after formation of compound nucleus (CN). Fission before CN formation is known as quasi-fission (QF) whereas fission after CN formation is called fusion-fission (FF). Presence of quasi-fission significantly reduces the CN formation probability and hence formation of heavier nuclei. QF is highly dependent on entrance channel parameters [1] and hence it is very important to study QF in order to choose optimum target-projectile combination. Experimentally, it is not easy to differentiate between QF and FF except for few distinguishing signatures. QF generally gives rise to higher fission fragment angular anisotropy [2], wider fission fragment mass distribution and/or fission fragment mass angular correlation [3], reduced ER cross sections, lower pre-scission particle multiplicity etc.

To study the fusion-fission dynamics in mass 200 region we performed an experiment, measuring fission fragment mass distributions for the system $^{16}O+^{184}W$, leading to CN $^{200}Pb^*$ at few energy points. ^{200}Pb CN was earlier studied at IUAC by measuring evaporation residue spin distributions. The experiment was performed at IUAC using pulsed beam with repetition rate of 250 ns. The target of enriched ^{184}W, with thickness 100 μg/cm^2 and a carbon backing of 30 μg/cm^2, was prepared at IUAC target laboratory, using the vacuum evaporation technique. The experiment was carried out in the General Purpose Scattering Chamber (GPSC), using two large area multi-wire proportional chambers (MWPC) (area 150×100 mm^2). The two MWPCs were placed on two arms of GPSC. The detector on the lower arm was placed at an angle of 50° and at a distance of 58 cm from the target. The distance between the detector on the upper arm and the target was kept at 39 cm. Angle of the detector on the upper arm was varied so that the two detectors were at folding angle. Two silicon surface barrier detectors (SSBD) were placed at angles of ±10° with respect to the beam direction. Two energy signals from MWPCs were fed to the ADC and 8 position signals from MWPCs along with two timing signals were fed to the TDC. The TDC was used in common start mode with start being "AND" between the beam pulse (RF) and the "OR" of both the MWPC timing signals. The two-dimensional (2D) spectrum between the MWPC timing signals separated fission fragments from other events. A 2D graphical cut was used to select only the fission events. The analysis was carried out to extract the mass widths for the reaction. The time of flight (TOF) was converted to mass ratio. Figure 4 shows the 2D plot of time of flight from both the detectors. Mass distribution at E_{lab}=96 MeV is shown in figure 5. These are preliminary results and further analysis is in progress.

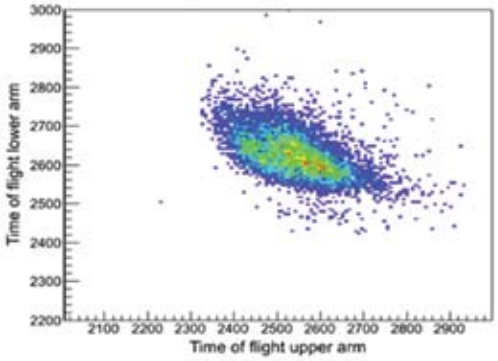

Fig.4. TOF from both MWPCs to identify fission events.

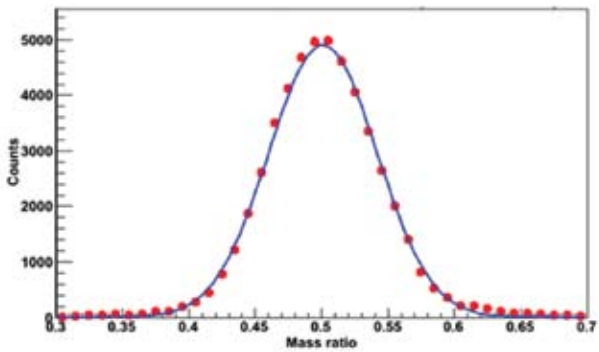

Fig. 5. Fission fragment mass distribution at E_{lab} = 96 MeV.

References

[1] A.C. Berriman *et al.,* Nature (London) **413**, 144 (2001).
[2] B.B. Back *et al.,* Phys. Rev. Lett. **50**, 818 (1983).
[3] R. Rafiei *et al.,* Phys. Rev. C **77**, 024606 (2008).

5.1.5 Fission Dynamics study in ^{243}Am and ^{254}Fm

K. Banerjee[1], T.K. Ghosh[1], P. Roy[1], A. Chowdhury[1], R. Pandey[1], C. Bhattacharya[1], S. Kundu[1], G. Mukherjee[1], T.K. Rana[1], S. Bhattacharya[1], G. Mohanto[2], R. Dubey[2], N. Saneesh[2], P. Sugathan[2], R. Guin[3], S. Das[3] and P. Bhattacharya[4]

[1]Variable Energy Cyclotron Centre, 1/AF Bidhan Nagar, Kolkata 700064, India
[2]Inter University Accelerator Centre, Aruna Asaf Ali Marg, New Delhi 110067, India
[3]Radio Chemistry Division, Bhabha Atomic Research Centre, Mumbai 400085, India
[3]Saha Institute of Nuclear Physics, 1/AF Bidhan Nagar, Kolkata 700064, India

Two experiments were performed using ^{11}B beam, from the Pelletron facility of IUAC, New Delhi, on ^{232}Th and ^{243}Am targets. Beam energies used varied from 52 - 74 MeV. The motivation for the experiment was to study the fission dynamics at near barrier energies for ^{243}Am and ^{254}Fm systems. The entrance channel mass asymmetries for ^{11}B + ^{232}Th and ^{11}B + ^{243}Am systems are higher than their respective mass asymmetries at the Businaro-Gallone point. Therefore, we can expect compound nuclear fission process in these two cases. However, earlier measurement of angular distribution showed the presence of non-equilibrium fission process in these two systems [1,2].

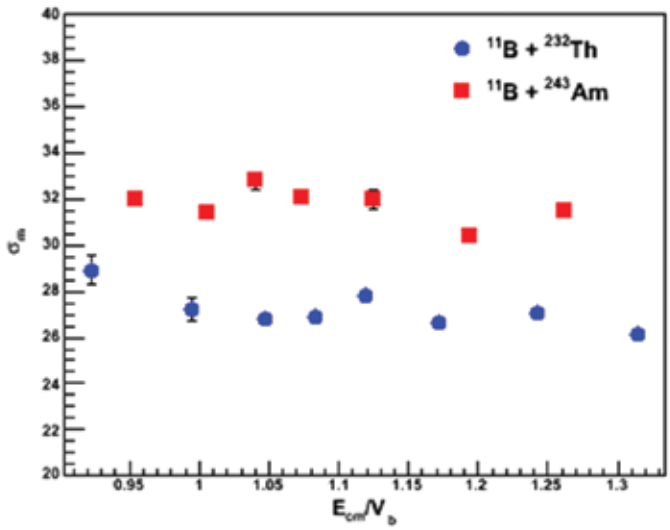

Fig. 6. Width of fission fragment mass distribution as a function of $E_{c.m.}/V_b$.

The present experiment was performed using two multi-wire proportional counters (MWPC, 20 cm × 6 cm) and four liquid scintillator based neutron detectors. MWPCs were kept at folding angle to detect fission fragments. Neutron detectors were kept at 30°, 60°, 90° and 120° with respect to the beam direction and at a distance of 1 m from the target position. Fission fragment mass distributions were extracted from fission fragment time of flight data. Mass distributions at different energies were fitted with Gaussian distribution function. Widths of the Gaussian fitting as a function of $E_{c.m.}/V_b$, are shown in figure 6. Here $E_{c.m.}$ is the centre of mass energy and V_b is the Coulomb barrier. The distribution is found to be flat in nature and there is no significant departure at below barrier energies. This signifies quasi-fission is absent in both the systems in the measured energy range. Further analysis, including neutron data, is under progress.

References

[1] B. K. Nayak *et. al.*, Phys. Rev. C **62**, 031601R (2000).
[2] R. Tripathi *et. al.*, Phys. Rev. C **75**, 024609 (2007).

5.1.6 The study of $^{12}C(\alpha,\gamma)$ astrophysical reaction using $^{12}C(^{6}Li,d)$ and $^{12}C(^{7}Li,t)$ reaction at 20 MeV

S. Adhikari[1], C. Basu[1], P. Sugathan[2], A. Jhingan[2], B.R. Behera[3], N. Saneesh[2], G. Kaur[3], M. Thakur[3], R. Mahajan[3], R. Dubey[2] and A.K. Mitra[1]

[1]Nuclear Physics Division, Saha Institute of Nuclear Physics, 1/AF Bidhan nagar, Kolkata 700064, India

[2]Inter University Accelerator Centre, Aruna Asaf Ali Marg, New Delhi 110067, India

[3]Department of Physics, Panjab University, Chandigarh 160014, India

The alpha transfer reactions *viz.* $^{12}C(^{6}Li,d)$ [1] and $^{12}C(^{7}Li,t)$ [2,3] at various incident energies have been used to determine the reduced alpha width of ^{16}O states. A comparison of the measured angular distributions with respect to an appropriate calculation yields the alpha spectroscopic factor (S_α). The alpha spectroscopic factor can be used to obtain the ANC if the reaction is peripheral. In the potential model, $^{12}C(\alpha,\gamma)$ E2 S-factor to the ground state depends on the ANC of the 6.92 MeV state and the alpha spectroscopic factor of the ground state. The determination of S_α, however, depends critically on the model used to analyse the data. In earlier calculations, the Finite Range Distorted Wave Born Approximation (FRDWBA) has been used assuming a direct alpha transfer process. However, $^{6,7}Li$, being loosely bound nuclei, are likely to breakup and can affect the transfer process and thereby, the S_α. This can be investigated in the framework of the Continuum Discretized Coupled Channel (CDCC-CRC) theory. In two separate experiments angular distributions were measured for the $^{12}C(^{6,7}Li,d/t)$ reactions at 20 MeV populating the discrete states of ^{16}O. The analysis of the $^{12}C(^{6}Li,d)$ reaction indicated the effect of very strong breakup coupling for the population of the ^{16}O ground state. In this respect, the analysis of the $^{12}C(^{7}Li,t)$ reaction is interesting because ^{7}Li has a higher breakup threshold (2.47 MeV) in comparison to ^{6}Li (1.46 MeV). As such whether breakup influences the angular distributions as for ^{6}Li is one of the motivations of this investigation.

The experiment was carried out using the General Purpose Scattering Chamber (GPSC) facility of IUAC, New Delhi. A $^{7}Li^{3+}$ beam at 20 MeV was bombarded onto a 200μg/cm^2 ^{12}C self-supporting target in the scattering chamber. Three ΔE-E silicon telescopes each 200-2000 μm were setup to perform the angular distribution measurements at 18°-124° in the laboratory. The average beam current was about 15-20 nA. The triton angular distributions measured in $^{12}C(^{7}Li,t)$ reaction at 20 MeV populating the ground state of ^{16}O is shown in figure 7(a). In figure 7(b), we show the measured energy spectrum for the $^{12}C(^{7}Li,t)^{16}O^*$ reaction at 40°. The energies of the discrete states of ^{16}O populated in the reaction are marked in the figure. The direct alpha transfer process is calculated using the FRDWBA formalism in FRESCO. This calculation is shown by black line in the figure. The alpha spectroscopic factor in this calculation is assumed to be 1. It is clear that the FRDWBA calculations are unable to explain the observed angular distributions. The CDCC-CRC calculations are then performed and shown by the red line. It is now seen that the inclusion of breakup coupling in the calculation improves the agreement significantly. This is a similar observation as in the $^{12}C(^{6}Li,d)$ reaction at 20 MeV. The BIT mechanism is thus found to be significant for the $^{12}C(^{7}Li,t)^{16}Ogs$ reaction. The spectroscopic factor using CDCC-CRC theory for the $^{12}C(^{7}Li,t)$ is 0.25 and that from $^{12}C(^{6}Li,d)$ is $0.1^{+0.09}_{-0.06}$.

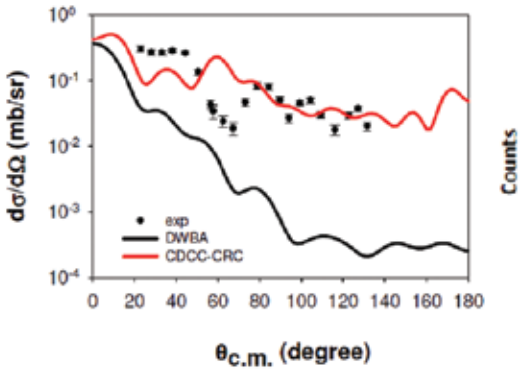

Fig. 7(a). Triton angular distributions in $^{12}C(^{7}Li,t)$ reaction at 20 MeV.

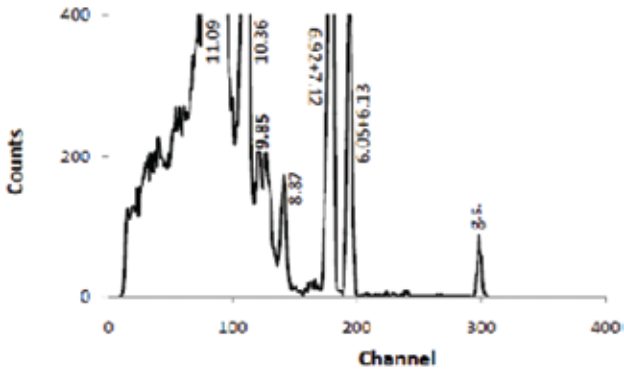

Fig. 7(b). Measured energy spectrum for the $^{12}C(^{7}Li,t)^{16}O^{*}$ reaction at 40°.

References

[1] S. Adhikari, C. Basu, I.J. Thompson, P. Sugathan, A. Jhingan *et al.,* AIP Conference Proceedings 1491, 359 (2012).
[2] N. Oulebsir *et al.,* Phys. Rev. C 85, 035804 (2012).
[3] S. Adhikari, C. Basu, P. Sugathan, A. Jhinghan *et al.,* EPJ Web of Conferences (communicated).

5.1.7 Lifetime measurements in ^{175}Re

Aman Rohilla[1], C.K. Gupta[1], Indu Bala[2], R.P. Singh[2], S. Muralithar[2], Siddharth Roy[3], Ashok Kumar[4], I.M. Govil[4], H.P. Sharma[5], Saikat[5] and S.K. Chamoli[1]

[1]Department of Physics and Astrophysics, University of Delhi, Delhi 110007, India
[2]Inter University Accelerator Centre, Aruna Asaf Ali Marg, New Delhi 110067, India
[3]Department of Physics, Visva Bharati, Santiniketan 731204, India
[4]Department of Physics, Panjab University, Chandigarh 160014, India
[5]Department of Physics, Banaras Hindu University, Varanasi 221005, India

Odd- Z nuclei having mass A~175 shows different nuclear structure phenomena which can be understood by studying the properties of the single particle orbits that have shape-driving effects in γ-soft nuclei [1,2]. Nuclei in the above mentioned mass region are normally found to have deformed prolate structures in their ground state, but, when they are excited to high spins by high excitation energy, they assume different shapes depending on the type of orbitals occupied by the valence nucleons. In this mass region, low Ω and high j intruder orbitals come into play which are down-slopping orbitals in the Nilsson diagram and thus take the nucleus to the positive deformation side which causes the nucleus to assume prolate shape. In the case of neutron deficient Re nuclei, there have been predictions of co-existence between different prolate configurations [3,4]. When the odd proton acquires down-slopping orbits, it has a strong polarizing effect on the even-even soft nuclear core giving rise to nuclear shape changing to deformed nuclear structure. As the deformation affects the energy of the whole band, it causes the band crossing frequencies corresponding to the alignment of $i_{13/2}$ neutron pair to shift to higher values. To study the variation in nuclear shape as a function of excitation energy and spin we have performed the lifetime measurements for different quasi-proton bands in ^{175}Re isotope through the recoil distance Doppler shift method (RDM) [5]. The level scheme related to this work exists already [6]. The measured transition rates may provide important information about the configuration dependent shapes of the Re nuclei.

The high spin states of 175Re were populated using the heavy ion fusion reaction $^{165}Ho(^{16}O,6n)$ ^{175}Re at beam energy of 107 MeV, provided by the 15UD Pelletron at IUAC, New Delhi. The experiment was performed using 3 Clover detectors without Compton-suppression and 2 HPGe detectors having Compton suppression in the GDA array of IUAC. The minimum distance between the target and stopper is measured using the capacitance method [7]. The data were taken at 16 target-stopper distances ranging from 10 – 7000 μm. Data acquisition was done using the online data sorting program CANDLE at IUAC. The data

were acquired in singles with the hardware coincidence between any of the Ge detectors and any two of the 14-element BGO multiplicity filter. Excitation function was carried out in the energy range 96 - 107 MeV. Singles spectra obtained were then compared. This revealed that, in addition to our nuclei of interest, other nuclei were also populated which made the excitation function experiment difficult for producing ^{175}Re. Data obtained in the detectors at the same angle, after calibration and gain matching, were added together to get the raw spectrum. The detailed analysis is in progress.

References

[1] W. Nazarewicz *et al.,* Nucl. Phys. A 512, 125 (1990).
[2] C.H. Yu *et al.,* Nucl. Phys. A 511, 157 (1990).
[3] R.A. Bark *et al.,* Nucl. Phys. A 501, 157 (1989).
[4] R. Bengtsson, Nucl. Phys. A 520, 201c (1990).
[5] T.K. Alexander, in Advances in Nuclear Physics, edited by M. Baranger and E. Vogt (Plenum, New York, 1978), Vol. 10, p. 197.
[6] T. Kibedi *et al.,* Nucl. Phys. A 539, 137 (1992).
[7] T.K. Alexander and A. Bell, Nucl. Instrum. Meth. 81, 22 (1970).

5.1.8 RDM Plunger facility test with Clover detectors

Aman Rohilla[1], C.K. Gupta[1], Indu Bala[2], R.P.Singh[2], S. Muralithar[2] and S.K. Chamoli[1]

[1]Department of Physics and Astrophysics, University of Delhi, Delhi 110007, India
[2]Inter University Accelerator Centre, Aruna Asaf Ali Marg, New Delhi 110067, India

The lifetime measurement of the transitions of the excited nuclear states provides valuable information for the nuclear structure of the nucleus. The transition probabilities obtained from level lifetimes give direct information about the wave function of the two states involved in the electromagnetic decay of the nucleus. Therefore, level lifetimes give information about the equilibrium shape of the nucleus and also the changes taking place in the nuclear shape at high spin and excitation energy. So, the method of lifetime measurement has been used to resolve a number of structural issues in nuclei. The recoil distance measurement (RDM) is one of the techniques for the measurement of lifetimes in the range of few nanoseconds to picoseconds [1]. For the measurement of lifetime, the plunger set-up, present at IUAC, has been used in conjunction with Gamma Detector Array (GDA) [2]. In the present experimental activity, our aim was of two fold; one to check the consistency and precision of three DC motors of the RDM plunger set-up, and the other was to compare the quality of data obtained with Compton-suppressed HPGe detectors and unsuppressed Clover detectors.

For this experiment, the heavy ion fusion reaction ^{94}Zr(^{12}C, 4n)^{102}Pd was used. The beam energy of 67 MeV was provided by the 15UD Pelletron accelerator of IUAC. The target foil consisted of a thin layer of ^{94}Zr (thickness ~500 μg/cm^2), which was evaporated on a Ta foil (thickness ~4 mg/cm^2). A thin layer of ^{197}Au (thickness ~40 μg/cm^2) was used to protect the Zr layer from oxidation. The stopper foil was ^{197}Au of thickness ~ 8 mg/cm^2, which was made by rolling. The minimum distance of ~8 μm was achieved in between the target and the stopper using the capacitance method [3]. To detect the de-excited γ-rays, five γ-detectors (two HPGe with Compton-suppression and three Clovers without suppression) were used in GDA. One HPGe detector with suppression and three Clovers were used in the backward ring at 144° and the remaining HPGe detector was used in the forward ring at 51° of the old GDA structure. Some transitions like 332 keV, 556 keV, 719 keV and 836 keV for ^{102}Pd were observed in this facility test spanning four shifts. This experimental activity was also reported in the DAE symposium 2013 [4].

References

[1] T.K. Alexander, in Advances in Nuclear Physics, Vol. 10, Plenum press, New York (1968), page 197.
[2] S. K. Chamoli, "Nuclear structure studies at high spins" (LAP LAMBERT Academic Publishing, GmbH & Co. KG, 2012) p. 108.
[3] T.K. Alexander and A. Bell, Nucl. Instru. Meth. 81, 22 (1970).
[4] A. Rohilla *et al.,* Proceedings of the DAE Symp. on Nucl. Phys. 58, 946 (2013).

5.1.9 High spin spectroscopy in ^{105}Cd

M. Kumar Raju[1,2], D. Negi[3], S. Muralithar[1], R.P. Singh[1], R. Kumar[1], Indu Bala[1], T. Trivedi[4], A. Dhal[5], K. Rani[1], R. Gurjar[1], D. Singh[6], J. Kaur[7], R. Palit[8], B.S. Naidu[8], S. Saha[8], J. Sethi[8] and R. Donthi[8]

[1]Inter University Accelerator Centre, Aruna Asaf Ali Marg, New Delhi 110067, India
[2]Nuclear Physics Department, Andhra University, Visakhapatnam 530003, India
[3]Department of Nuclear Physics, iThemba LABS, 7129, South Africa
[4]Guru Ghasidas Vishwavidyalaya, Bilaspur 495009, India
[5]Department of Particle and Astrophysics, Weizmann Institute of Science, Rehovot 76100, Israel
[6]Department of Physics, Central University of Jharkhand, Ranchi 835 205, India
[7]Department of Physics, Punjab University, Chandigarh 160014, India
[8]Tata Institute of Fundamental Research, Mumbai 400005, India

Study of transitional nuclei with Z~50 and mass ~105 is interesting due to existence of various structural phenomena. This is due to the presence of proton holes below the Z= 50 shell gap and neutron particles above the N = 50 shell gap, which can couple in various modes giving rise to complex structures with increasing angular momentum. For example, lighter cadmium isotopes are predicted to have rapid shape transitions as a function of rotational frequency due to the occupation probability of valance quasi-particles in deformation driving high-J, low-Ω orbitals. Such a shape transition is evident in ^{103}Cd [1] based on total Routhian surface calculations (TRS), which depict that, the prolate shape of this nucleus persists up to spin J^{π} =39/2− and changes to an oblate shape at higher spin. On the other hand, in case of ^{107}Cd [2], the shape of the nucleus is quite γ-soft at low spin and evolves to a near prolate shape at higher rotational frequencies.

In the present experiment, high spin states in ^{105}Cd were populated using the fusion evaporation reaction ^{92}Mo(^{16}O, 2pn)^{105}Cd at an incident beam energy of 75 MeV. Beam of ^{16}O ions with current of 1 pnA was delivered by the 14UD Pelletron accelerator at TIFR, Mumbai. The target, used in the experiment, was of 1 mg/cm^2 thickness with 10 mg/cm^2 Au backing. The de-exciting γ-rays were detected using the Indian National Gamma Array (INGA) [3] facility at TIFR. During this experiment, INGA comprised of fifteen Compton suppressed Clover Ge detectors, out of which, four were at 90o, two at 40°, two at 65°, two at 115°, two at 140° and the remaining three were at 157°, with respect to the beam direction.

The coincidence data were collected in list mode with digital data acquisition system [4], using Pixie-16 Module by XIA-LLC software. A total of more than two billion two or higher fold coincident events were recorded. The measured coincident events were then sorted in to Eγ-Eγ symmetric matrix having dimensions 4k×4k. This matrix set was

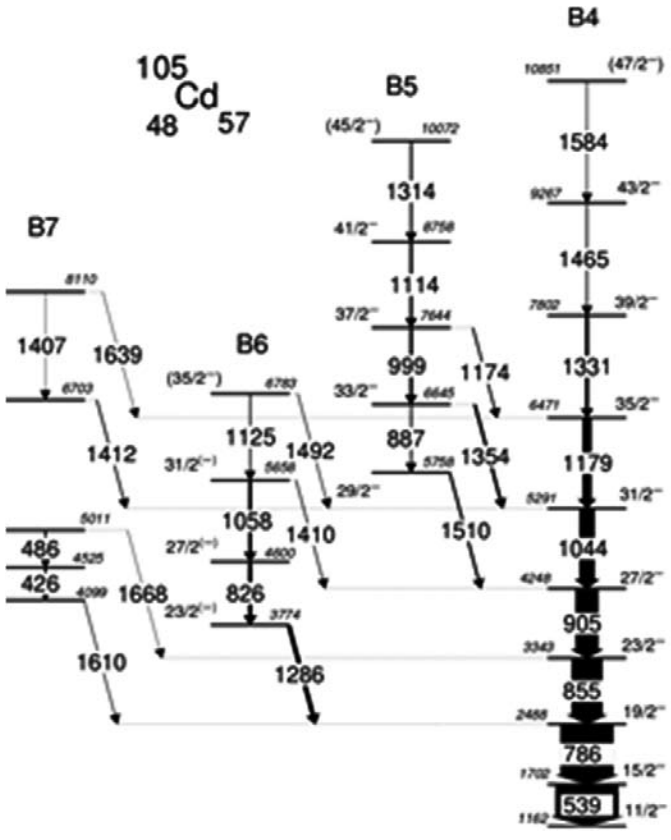

Fig.8: Partial level scheme of 105Cd.

analyzed using RADWARE [5] program for the construction of level scheme. An angle dependent matrix 90° vs 157° was constructed for assigning the multi-polarity of the γ-transitions based on conventional DCO technique.

In the present work, the level scheme of ^{105}Cd was examined. It fits well with the previously reported level scheme reported in Ref.[3], except for few levels in negative and positive parity bands. We have placed 30 new transitions in the level scheme based on coincidence and intensity arguments. Figure 8 shows the partial level scheme of ^{105}Cd with the newly identified negative parity band structures (band B5, B6 and B7) deduced in the present work. A representative γ− γ coincidence sum spectrum, gated on 539 and 786 keV, showing the transitions in negative parity bands B4, B5, B6 and B7 can be found in figure 9.

Band B4 was the strongly populated band, proposed to have $\nu h_{11/2}$ band head configuration. In this work, this band is observed up to a spin $J^{\pi} = (47/2^{-})$ and excitation energy ~10.8 MeV and agrees well with the reported levels in previous work [2]. Band B5 is a new negative parity sequence identified in the present work, which consists of 887, 999, 1114 and 1314 keV in-band transitions. This band is decaying to the negative parity states in band B4 via linking transitions of energies 1510, 1354, and 1174 keV. The observed R_{DCO} of 887, 999, 1114 keV γ-ray transitions are consistent with E2 nature, suggesting $J^{\pi} = 33/2^{-}$, $35/2^{-}$ and $39/2^{-}$, respectively. The present work also established a negative parity band B6 built on $23/2^{-}$ state at 3774 keV, decaying to the yrast negative parity band B4 via a new 1286 keV transition. This band is extended to a spin 35/2 with the addition of three γ-transitions of energies 826, 1058 and 1125 keV.

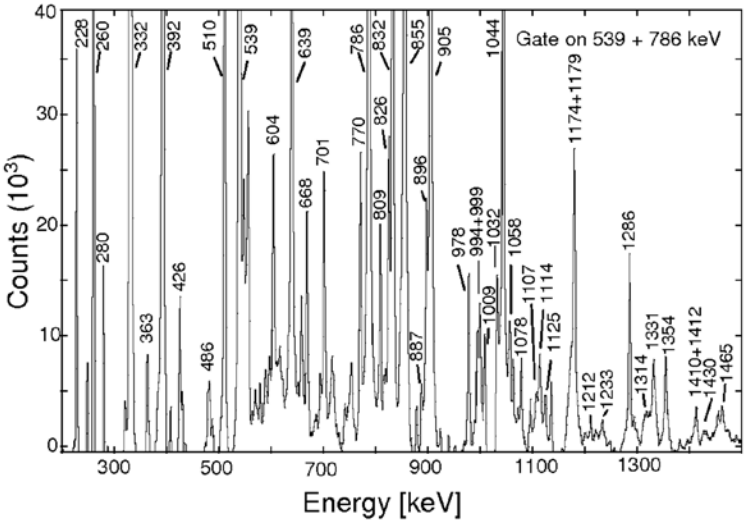

Fig.9: Sum spectrum gated on 539 + 786 keV showing the transitions in band B4, B5, B6 and B7 of ^{105}Cd.

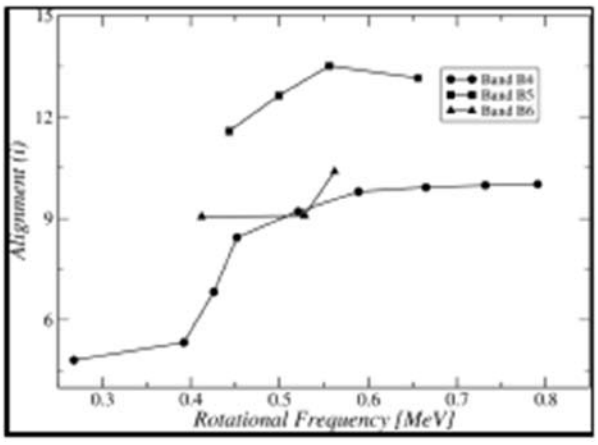

Fig.10: Alignment as a function of rotational frequency.

Figure 10 shows the alignments observed with respective to rotational frequency in negative parity sequences. The first band crossing for band B4 has been observed around the rotational frequency ≈ 0.43 MeV. The observed alignment in this band is smooth and it is interpreted due to the breaking of $\nu(g_{7/2})^2$ pair [2]. After the first band crossing, the $\nu h_{11/2}$ $\nu(g_{7/2})^2$ configuration coupled to a pair of $\pi g_{9/2}$ proton holes generates the high spin states in band B4. Bands B5 and B6 are the excited bands based on the configurations involving ground state negative parity band. Further data analysis and microscopic calculations are in progress to understand the nature of the observed negative parity bands and newly identified positive parity bands.

References

[1] A. Chakraborty *et al.,* Phys. Rev. C 76, 044327 (2007).
[2] Dan Jerrestam *et al.,* Nucl. Phys. A 593, 162 (1995); Nucl. Phys. A 545, 835 (1992).
[3] R. Palit, AIP Conf. Proc. 1336, 573 (2011).
[4] R. Palit *et al.,* Nucl. Instrum. Meth. A 680, 90 (2012).
[5] D.C. Radford, Nucl. Instrum. Meth. A 361, 297 (1995).

5.1.10 Study of shears mechanism at low deformation in ^{105}In

T. Trivedi[1,2], D. Negi[3], M. Kumar Raju[1], S. Muralithar[1], R.P. Singh[1], R. Kumar[1], Indu Bala[1], K. Rani[1], R. Gurjar[1], A. Dhal[4], D. Singh[5], R. Palit[6], B.S. Naidu[6], S. Saha[6], J. Sethi[6], R. Donthi[6] and S. Jadhav[6]

[1]Inter University Accelerator Centre, Aruna Asaf Ali Marg, New Delhi 110067, India
[2]Guru Ghasidas Vishwavidyalaya, Bilaspur 495009, India
[3]Department of Nuclear Physics, iThemba LABS, 7129, South Africa
[4]Department of Particle and Astrophysics, Weizmann Institute of Science, Rehovot 76100, Israel
[5]Department of Physics, Central University of Jharkhand, Ranchi 835 205, India
[6]Tata Institute of Fundamental Research, Mumbai 400005, India

In recent years, nuclear states decaying by fast M1 transitions forming a band in A ~110 region have been the topic of intensive investigations. Similar sequences, first discovered in ^{199}Pb and later in other odd-N Pb [1] isotopes, were explained by the Tilted Axis Cranking (TAC) model [2] due to magnetic rotation in nuclei. The mechanism of spin generation within the band is by the 'shears mechanism'. Such tilted solutions are expected to be present in various parts of the nuclear chart in the vicinity of magic numbers, where nuclear deformation is low. Magnetic rotation has been extensively studied in A~110 region in Cd, Ag and Sn isotopes. Often the shears mechanism is accompanied by a small rotational contribution of core in the spin generation. *A priori* it is not known whether the TAC model, which requires a deformed mean field, would be able to describe such states. In order to extend the study of magnetic rotation phenomenon in low deformed states, lower mass In isotopes with few nucleons outside the doubly magic Sn core are good candidates. Many $\Delta I = 1$ M1 sequences are known in these low mass (A<107) In isotopes. Preliminary results of the present investigations are reported here.

High spin states of ^{105}In nucleus have been populated via the ^{92}Mo(^{16}O, 3n)^{105}In reaction at an incident beam energy of 75 MeV. The ^{16}O beam was delivered by the 14UD Pelletron accelerator of TIFR, Mumbai. The γ-rays emitted in the reaction have been measured with the INGA which is a Compton suppressed Clover detector array with a provision of placing 24 Clovers: 3 at 23°, 40°, 65°, 115°, 140°, 157° and 6 at 90° with respect to the beam direction [3]. In the present experiment, 16 Clover detectors were used at various angles. The distance between the target and the detector was ~25 cm. Two and higher fold Clover coincidence events were recorded in a fast digital data acquisition system based on Pixie-16 modules of XIA-LLC. The target consisted of ~1 mg/cm^2 isotopically enriched ^{92}Mo on a gold backing. The

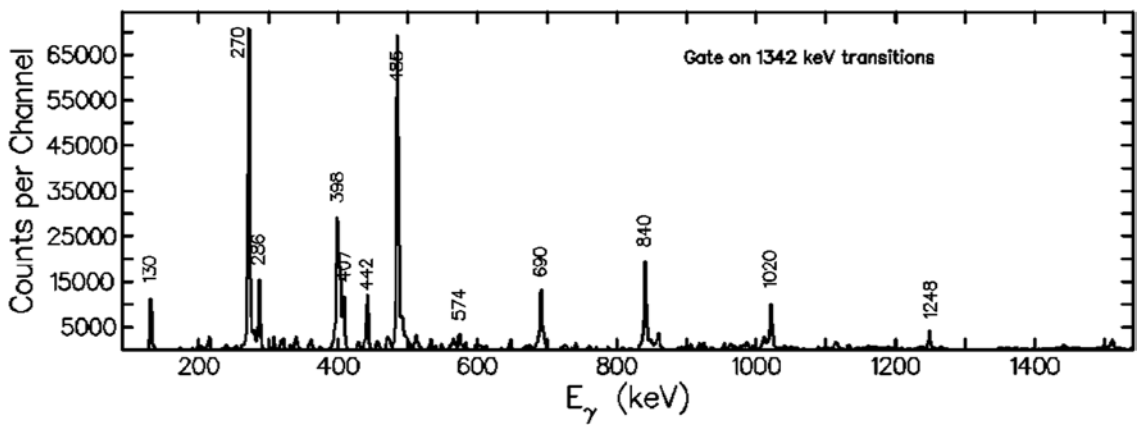

Fig. 11. Identified transitions from different bands of ^{105}In.

data sorting routine "Multi-pARameter time-stamp based COincidence Search program" (MARCOS), developed at TIFR, sorts the time-stamped data to generate one-dimensional histograms, *Eγ-Eγ* matrices. The coincidence events were sorted into the conventional γ-γ symmetric as well as asymmetric matrices. The software package RADWARE and DAMM were used for the data analysis. The transitions reported in the level scheme developed by D. Kast *et al.* [4] were identified and used as reference data for this measurement. For identifying the transitions of different bands of ^{105}In, gated spectra with gate on 1342 keV γ-ray are shown in figure 11. The gated spectrum depicts the 485-272–840–407-286 keV cascade of yrast band as well as 130-398-690-442 keV cascade of dipole band.

Lineshapes of magnetic dipole band have been identified and lifetimes of these states have been measured by Doppler shift attenuation method (DSAM). For analyzing the line shapes of different transitions of ^{105}In, the LINESHAPE program was used. Lifetimes of levels were obtained from the analysis of line shapes in the detectors at 157° and 23°. The observed line shapes were obtained by gating below the transition of interest. The initial results of line shapes and their simulated line shapes for the 442 and 691 KeV transitions, for ΔI = 1 band are shown in figure 12.

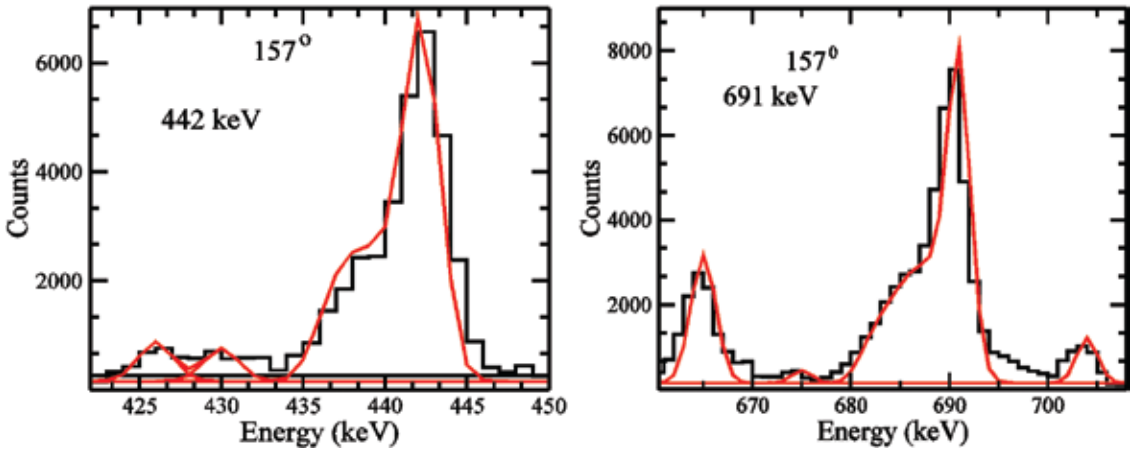

Fig. 12. Experimental and theoretical line shapes for 442 keV and 691 keV transitions in the positive parity band of ^{105}In at θ = 157o.

The directional correlation of oriented states (DCO) and integrated polarization direction correlation (IPDCO) analysis is in progress to determine the spin and parity of different states. Further, in order to distinguish between electric and magnetic character, multi-polarity assignments will be done by extracting γ-ray linear polarizations using 90° detectors. This can be achieved by considering the four crystals within a single Clover detector of the INGA spectrometer as Compton parameters. Detailed analysis is in progress.

References

[1] H. Hubel, Prog. Part. Nucl. Phys. 54, 1 (2005).
[2] S. Frauendorf, Rev. Mod. Phys. 73, 463 (2001).
[3] R. Palit, AIP Conf. Proc. No. 1336 (AIP, New York, 2011), p. 573.
[4] D. Kast *et al.,* Eur. Phys. Jour. A 3, 115 (1998).

5.1.11 Chirality in nuclei

D. Tonev[1], M.S. Yavahchova[1], N. Goutev[1], G.de Angelis[2], P. Petkov[1], R.K. Bhowmik[3], R.P. Singh[3], S. Muralithar[3], N. Madhavan[3], R. Kumar[3], M. Kumar Raju[4], J. Kaur[5], G. Mohanto[3], A. Singh[5], N. Kaur[5], R. Garg[6], A. Sukla[7], Ts. K. Marinov[1] and S. Brant[8]

[1] Bulgarian Academy of Sciences, Institute for Nuclear Research and Nuclear Energy, Sofia, Bulgaria
[2] INFN, Laboratori Nazionali di Legnaro, Legnaro, Italy
[3] Inter University Accelerator Center, Aruna Asaf Ali Marg, New Delhi 110067, India

[4] Nuclear Physics Department, Andhra University, Visakhapatnam 530003, India
[5] Department of Physics, Punjab University, Chandigarh 160014, India
[6] Department of Physics and Astrophysics, Delhi University, Delhi 110007, India
[7] Department of Physics, Banaras Hindu University, Varanasi 221005, India
[8] Department of Physics, Faculty of Science, Zagreb University, Zagreb, Croatia

Chirality is a phenomenon which is often found in nature. Examples of systems demonstrating chirality are present in chemistry, biology, high energy physics etc. Does chirality exist in nuclear physics? It is a novel feature of rotating nuclei which is among the most studied phenomena during the recent years. A spontaneous breaking of the chiral symmetry can take place for configurations where the angular momenta of the valence protons, valence neutrons, and the core are mutually perpendicular [1]. The main goal of the present work was to check for the existence of chirality in the mass region A~ 100.

Excited states in ^{102}Rh were populated using the reaction ^{94}Zr(^{11}B,3n)^{102}Rh at a beam energy of 36 MeV. The beam was delivered by the 15UD Pelletron accelerator of IUAC, New Delhi [2][3]. The target consisted of 0.9 mg/cm^2 ^{94}Zr, enriched to 96.5%, evaporated onto a 8 mg/cm^2 gold backing. The recoils were leaving the target with a mean velocity v of about 0.9% of the velocity of light, *c*. The de-exciting γ-rays were registered by the INGA, whose 15 Clover detectors are accommodated in a 4π geometry [4]. For the purposes of the Doppler-Shift Attenuation Method (DSAM) analysis, the detectors of INGA were grouped into rings with approximately the same position with respect to the beam axis. The rings, where appreciable Doppler-shifts are observed, are at angles of 32°, 57°, 123° and 148° Gain matching and efficiency calibration of the Ge detectors were performed using ^{152}Eu and ^{133}Ba radioactive sources before sorting the data in matrices and cubes.

In order to investigate the level scheme and electromagnetic properties of the transitions of interest in ^{102}Rh, we have performed four types of data analyses. Such complex approach is employed for the first time in the case of the investigation of chirality in nuclei. The ordering of the transitions in the level scheme was determined according to γ-ray relative intensities, γ-γ coincidence relationships, and γ-ray energy sums. The electric or magnetic character and multi-polarity of the transitions were deduced by linear polarization and angular correlations measurements, respectively. We need to stress that the presently observed level scheme of ^{102}Rh is very rich and the information on the line shapes of consecutive transitions (i.e. effective lifetimes) was also used to construct the new Band 2 indicated in Figure 3.

The Doppler-shift attenuation method was utilized to determine the lifetimes of excited states in ^{102}Rh. The analysis was carried out within the framework of the Differential decay method (DDCM) [5] according to the procedure outlined in Ref. [6] where details about the Monte-Carlo simulation of the slowing down process, determination of stopping powers and fitting of line shapes can be found. For each level, lifetimes were derived independently at the four rings with appreciable Doppler-shifts. The lifetimes of the levels with I^{π} from $(11)^-_1$ to $(16)^-_1$ and from 10^-_2 to 11^-_2 have been deduced for the first time. More detailed information can be found in Ref. [7].

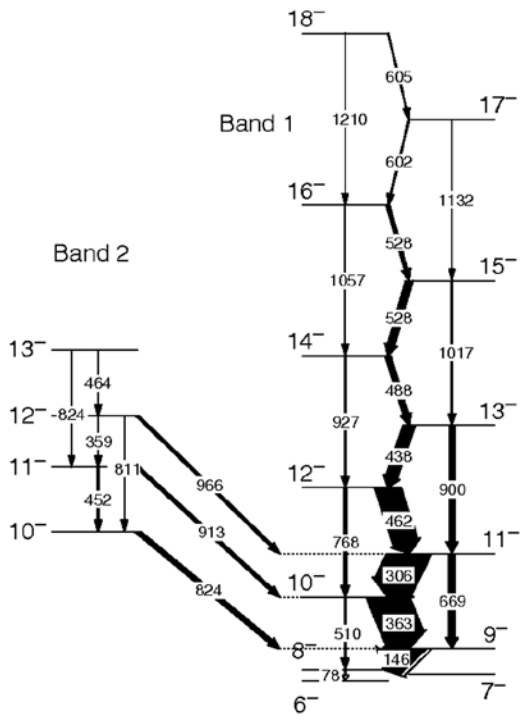

Fig. 13. Partial level scheme of ^{102}Rh. Two negative-parity bands, candidates for chiral partner bands, are indicated as Band 1 and Band 2.

In summary, our work presents for the first time in the A~100 mass region a unique data set providing information on electromagnetic transition strengths in both chiral candidate bands. Our lifetime measurements and the theoretical analysis do not support static chirality in ^{102}Rh. This means that the chirality in ^{102}Rh, if it exists, has mainly a dynamical character.

D.T. express his gratitude to Ivanka Necheva for her outstanding support. Thanks to the Pelletron staff of IUAC, New Delhi for their perfect work for our experiment. This research has been supported by Bulgarian Science Fund under contract DFNI-E 01/2 and by a NUPNET-NEDENSAA project funded by the Bulgarian Ministry of Education and Science. INGA was funded by the Department of Science and Technology, Government of India (No. IR/S2/PF-03/2003-I) and the University Grants Commission.

References

[1] S. Frauendorf and Jie Meng, Nucl. Phys. A 617, 131 (1997).
[2] G.K. Mehta and A.P. Patro, Nucl. Instr. Meth A 268, 334 (1988).
[3] D. Kanjilal *et al.,* Nucl. Instrum. Meth. A 328, 97 (1993).
[4] S. Muralithar *et al.,* Nucl. Instrum. Meth. A 622, 281 (2010).
[5] G. Bohm, A . Dewald, P. Petkov, P. von Brentano, Nucl. Instrum. Meth. A 329, 248 (1993).
[6] P. Petkov *et al.,* Nucl. Phys. A 640, 293 (1998).
[7] D. Tonev, M. S. Yavahchova, N. Goutev *et al.,* Phys. Rev. Lett. 112, 052501 (2014).

5.1.12 In-beam γ-ray spectroscopy of ^{127}I

S. Chakraborty[1], H.P. Sharma[1], P. Banerjee[2], S. Ganguly[3], A. Kumar[4], N. Kaur[4], S. Kumar[5], S. Muralithar[6], R.P. Singh[6], L. Chaturvedi[7], A. Kumar[1], A.K. Jain[8] and S Laxhminarayan[9]

[1]Department of Physics, Banaras Hindu University, Varanasi 221005, India
[2]Saha Institute of Nuclear Physics, 1/AF Bidhan Nagar, Kolkata 700064, India
[3]Department of Physics, Chandernagore College, Chandannagar 712136, India
[4]Department of Physics, Punjab University, Chandigarh 160014, India
[5]Department of Physics and Astrophysics, University of Delhi, Delhi 110007, India
[6]Inter University Accelerator Center, Aruna Asaf Ali Marg, New Delhi 110067, India
[7]Department of Pure and Applied Physics, Guru Ghasidas Vishwavidyalaya, Bilaspur 495009, India
[8]Department of Physics, Indian Institute of Technology, Roorkee 247667, India
[9]Department of Physics, Andhra University, Visakhapatnam 530003, India

Iodine nuclei are the representative of the transitional nuclei as they exist in between the spherical Sn (Z = 50) and the well deformed La (Z = 58) nuclei. As per the available data, the band structures of ^{127}I [1] are not well studied compared to the reported data on $^{113\text{-}125}$I [2,3]. Particularly, the information on spin and parity assignment is lacking in ^{127}I. Therefore, in-beam γ-ray spectroscopy of ^{127}I was planned to improve the information on band structure of ^{127}I [1].

In-beam γ-ray spectroscopy of ^{127}I was carried out using 15UD Pelletron accelerator [4] at IUAC, New Delhi via ^{124}Sn(^{7}Li, 4nγ)^{127}I fusion-evaporation reaction at 33 MeV by using enriched ^{124}Sn target. INGA with 15 Compton-suppressed Clover detectors was used [5] and about 2×10^{8} γ-γ coincidence events were collected by using CAMAC based data acquisition system. Offline data analysis was carried out using the computer code INGASORT [6]. Several matrices were formed by sorting of the gain matched list mode data to carry out the γ-γ coincidence, angular correlation and polarization analysis.

From this work, few new γ-transitions were placed in the level scheme of ^{127}I and the spins and parities of several levels have been confirmed from the angular correlation (R_{DCO}) and linear polarization (Δ^{IPDCO}) results obtained from this experiment.

On the basis of present results, a three quasi-particle band has been established at $21/2^+$ state, above 2806.3 keV [7] and $\pi g_{7/2} \otimes \nu h^2_{11/2}$ configuration has been proposed for this band on the basis of the systematic analysis of several characteristic features of the similar band reported in ^{123,125}I.

A cascade of $\Delta I = 1$ transitions with weak crossover transitions was reported [8] with tentative spin and parity assignments above 2901.2 keV level and tentatively assumed as a three quasi-particle band. The spin and parity of the band-head and levels above have been confirmed in the present investigation [9].

The $\pi h_{11/2}$ band has been extended up to $31/2^-$ by placing a 683.7 keV E2 γ-transition above 3958 keV level at $27/2^-$ [10]. The spin and parity of three levels of this band at 3958.0 keV, 4367.5 keV and 4641.7 keV have been confirmed in this work.

Two side feeding γ-transitions of 802.1 keV and 547.2 keV, decay to the $13/2^+$ and $17/2^+$ levels of $\pi g_{7/2}$ band [1] from the levels at 2068.4 keV and 2423.2 keV, respectively. The spins and parities of these two levels have been confirmed in the present study [11]. Several non-collective states are reported [1], however, spins and parities are not confirmed. From the present study, we are able to confirm the spins and parities of these levels also.

The authors are thankful to the staff of the target lab, Pelletron and INGA facilities at IUAC. The first author is also thankful to IUAC for providing the financial support vide project no. UFR-51321.

References

[1] B. Ding *et al.,* Phys. Rev. C 85, 044306 (2012).

[2] Hariprakash Sharma *et al.,* Phys. Rev. C 64, 064310 (2001).

[3] M. Gai *et al.,* Phys. Rev. C 26, 3 (1982).

[4] G.K. Mehta *et al.,* Nucl. Instrum. Meth. A 268, 334 (1988).

[5] S. Muralithar *et al.,* Nucl. Instrum. Meth. A 622, 281(2010).

[6] R.K. Bhowmik *et al.,* DAE Symp. Nucl. Phys. 44B (2001).

[7] S. Chakraborty *et al.,* DAE Symp. Nucl. Phys. 58 610 (2013).

[8] Y. H. Zhang *et al.,* Annual Report [01.04.2001 – 31.03.2002], Tandem Accelerator Center, Univ. of Tsukuba, Japan, p. 39.

[9] H.P. Sharma *et al.,* Proc. FIG12, IUAC, India (2012).

[10] S. Chakraborty *et al.,* AIP Conf. Proc. 1524, 117 (2013).

[11] Hariprakash Sharma *et al.,* DAE Symp. Nucl. Phys. 57 276 (2012).

5.2 MATERIALS SCIENCE

D. K. Avasthi

There were 56 user experiments utilizing swift heavy ions irradiation in materials science beamlines comprising of 175 shifts. Out of these experiments, 23 runs were BTA experiments associated with students' Ph.D. programmes. Most of the beam-times were performed in the irradiation chamber in the materials science beamline in beamhall-I while 2 experiments of over 12 shifts were performed in materials science beamline in beamhall-II. In some of the experiments online ERDA, online RGA, in-situ XRD and in-situ Raman facilities were utilized. Apart from these, there were large numbers of experiments in materials science beam line in low energy ion beam facility. Synthesis and modification of nanostructures remained as one of the key areas of investigations.

The in-situ Raman study of the rutile phase of titanium oxide was undertaken to investigate the softening and stiffening of phonons. In-situ XRD studies were performed to study the stoichiometry dependent radiation stability of $Gd_2Zr_2O_7$. In-situ I-V and C-V measurements were performed to study the electrical transport at the interface of n-Si and ZnS:TiO_2 under swift heavy ion irradiation. Ni nanostructure was synthesized by swift heavy ion irradiation. It is demonstrated that swift heavy ion irradiation of graphene results in annealing of defects at low fluences whereas defects are produced at higher fluence and interesting to note is that it retains significant crystallinity even at fluence of 10^{14} ion/cm^2 of 150 MeV Au ions. There is a volume expansion in crystalline as well as amorphous Ge under swift heavy ion irradiation. The effect of high energy heavy ion irradiation was investigated on Au/Fe alloy nanoparticles embedded in silica matrix. The formation of CoSb phases were studied by annealing of bilayer of Co/Sb and annealing of swift heavy ion irradiated bilayer. The formation of Ge nanostructures is studied by low energy ion irradiation. The synthesis of partially embedded Au nanoparticles is shown by low energy ion irradiation of thin Au film on glass substrate. The structural modifications were studied in $AgInSe_2$ under high energy ion irradiation. The magnetic and topographical properties of Fe-Ni alloy films were studied under 100 MeV Ag ion irradiation. The dielectric response of PMMA/$ZnFe_2O_4$ composite was studied under 400 keV Ar ion irradiation. The effect of swift heavy ion irradiation on the structural, optical and electrical properties of oxide films (WO_3 and MoO_3) were studied under swift heavy ion irradiation.

An international conference on nanostructuring by ion beam was organized at Jaipur. An international conference on 'SHIMEC' and an international school on ion beams in materials science is planned in October 2014.

5.2.1 Softening and Stiffening of Phonons in Rutile Titanium Dioxide Film by Energetic Ion Irradiation

Subodh K. Gautam[1], Fouran Singh[1], I. Sulania[1], R.G. Singh[2], P.K. Kulriya[1], and E. Pippel[3]

[1]Mat. Science Group, Inter University Accelerator Centre, Aruna Asaf Ali Marg, New Delhi - 110067, India.
[2]Department of Physics, Bhagini Nivedita College, Delhi University, Delhi - 110043, India
[3]Max Planck Institute of Microstructure Physics, Weinberg 2, D-06120 Halle, Germany

Titanium dioxide (TiO_2) has wide interest in fundamental understanding of phase transition and the response of their physio-chemical properties due to changes in the crystallite size, and stoichiometry [1]. It is also known that TiO_2 is very susceptible to change in lattice parameters, which affects the whole lattice dynamics of the materials. Therefore, the study of phonon structure and their dispersion is essential to develop any device based on TiO_2. Hence, studies under irradiation using 120 MeV Ag was carried out and the softening and stiffening of phonons in rutile titanium dioxide films are investigated by *in situ* micro-Raman studies during energetic ion irradiation. The *in situ* study minimized other possible mechanisms of phonon dynamics and provides more authentic data. Results show that as the size decreases from 50 to 40 nm at initial fluences of irradiations, while A_{1g} mode shows softening of about 3 cm^{-1} along with increase in peak width. However, a further decrease in the size leads to the stiffening of this mode even upto the size of about 15 nm. Initial softening and broadening of Raman shift is attributed to the phonon confinement by structural defects and loss of stoichiometry [2]. The stiffening of A_{1g} mode is ascribed to large distortion of TiO_6 octahedra under the influence of lattice strain in the (110) plane, which gives rise to lengthening of equatorial Ti-O bond and shortening of apical Ti-O bond. The shortening of apical Ti-O bond induces stiffening of A1g mode in the framework of the Bond-Order-Length-Strength (BOLS) correlation mechanism [4]. According to this mechanism, the lattice periodicity is terminated with reduction in size and leads to the contraction of bonds between the surface atoms. The present experimental study also demonstrates the interplay between density of oxygen vacancies and strain in (110) surface in agreement with the prediction of the comprehensive first principle calculations [4]. The tensile strain induced by high density of oxygen vacancies in (110) plane leads to increase in the equatorial Ti-O bond length and shortening of apical Ti-O bond. Thus, the apical bond strengthened and gives rise to the stiffening of A_{1g} modes and reasonably well evidenced by the BOLS correlation mechanism. The size of ion tracks is estimated by fitting this equation and is found to be 1.81 ± 0.16 nm and is quite consistent with the value reported in literature [5]. Therefore, such studies could be useful for the fundamental understanding of multi-functional applications such as sensors, origin of d° magnetization of dilute magnetic semiconducting materials, catalysis and other surface related properties. Finally, it can also be concluded that energetic ions can be used efficiently for an in-depth understanding of the origin and dynamics of the phonon interactions. For details see [*Subodh K. Gautam et al J. Appl. Phys. 115 (2014) 143504*].

References

[1] A. Fujishima and K. Honda, Nature (London) 238 (1972) 37.

[2] Fouran Singh, R. G. Singh, Vinod Kumar, S. A. Khan, and J. C. Pivin, J. Appl. Phys. 110 (2011) 083520.

[3] Q. Sun, Prog. Solid State Chem. 35 (2007) 1.

[4] Da-Jun Shu, Shu-Ting Ge, Mu Wang, and Nai-Ben Ming, Phys. Rev. Lett. 101 (2008) 116102.

[5] Ken-ichi Nomura, Tetsuya Nakanishi, Yoshihiro Nagasawa, Yoshimichi Ohki, Koichi Awazu, Makoto Fujimaki, Naoto Kobayashi, Satoshi Ishii and Kunihiro Shima, Phys. Rev. B 68 (2003) 064106.

5.2.2 A Study on Dependence of Radiation Stability of $Gd_2Zr_2O_7$ on Stoichiometry

Renu Kumari[1], P K Kulriya[1], K. Saravanan[1], V. Gupta[2], A. K. Tyagi[2], D. K. Avasthi[1]

[1]Inter University Accelerator Centre, PO Box 10502, Aruna Asaf Ali Marg, New Delhi-110067

[2]Chemistry Division, Bhabha Atomic Research Centre, Mumbai-400085.

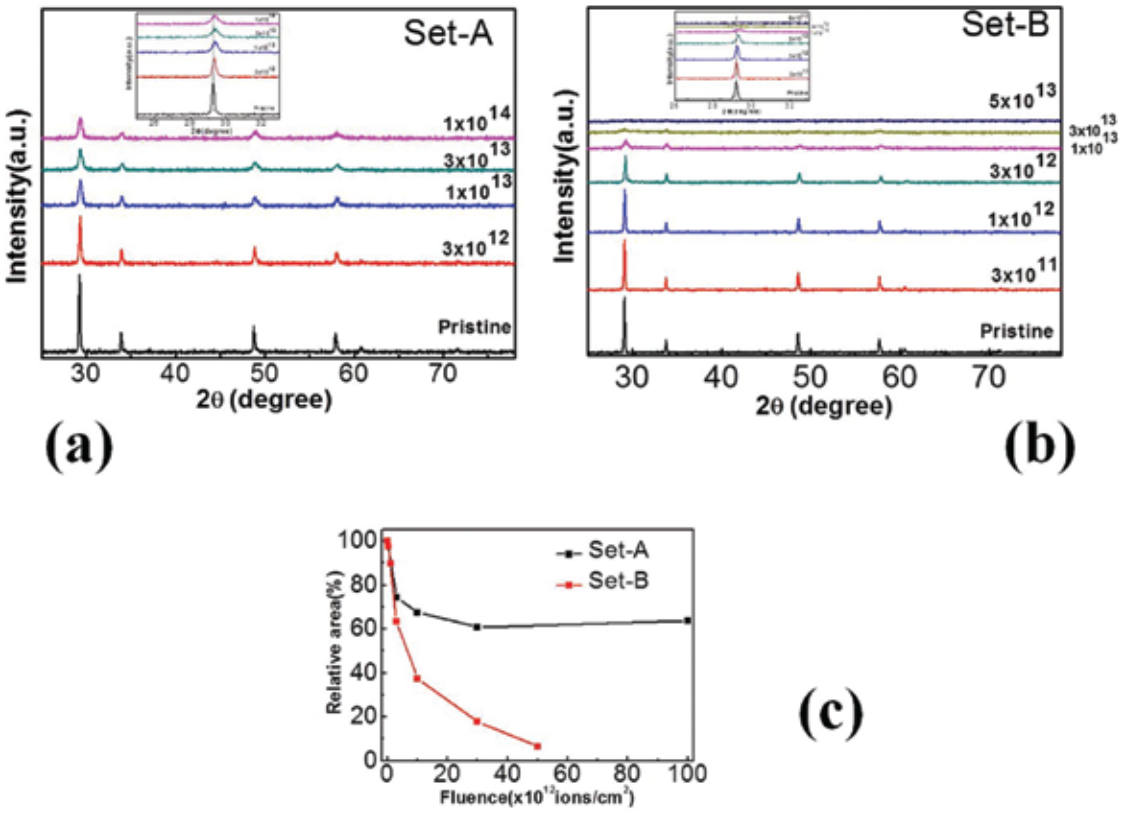

Fig. 14(a) and (b) *In-situ* XRD patterns recorded on set-A and set-B samples before and after irradiation with 120 MeV Au ions at the indicated fluences. The insets show expanded view of most intense peak. Fig.14(c) shows relative area under the most intense peak versus ion fluence of set-A and set-B with increasing fluence.

Ceramic oxides are promising materials for using them in extreme conditions such as high temperature and radiation environment etc. Pyrochlores with perfect $A_2B_2O_7$ stoichiometry are of great interest due to their capabilities for the incorporation of actinides (e.g. U, Np, Th, Pu, Am and Cm) generated from nuclear reactor[1], and waste immobilization or transmutation of actinides produced in nuclear power plants. The zirconates are found to be less perturbed by irradiation induced defects than the titanates[2,3]. $Gd_2Zr_2O_7$ is radiation tolerant material that can be used as host materials for radioactive wastes and actinides. The radiation resistance nature of $Gd_2Zr_2O_7$ can vary with change in stoichiometry. In present experiment, we have selected $Gd_2Zr_2O_7$ material named as set-A and set-B synthesised by two different methods. From resonant Rutherford backscattering spectrometry[4] (RRBS), we found out that stoichiometry of set-A matches with pyrochlore structure and stoichiometry of set-B deviates from pyrochlores structure ($A_2B_2O_7$). The samples (Set-A and set-B) were irradiated with 120-MeVAu ions for different fluences. The *in situ* X-ray diffraction (XRD) on these samples was performed at room temperature to study the stability of set-A and set-B under swift heavy ion irradiation. *In-situ* XRD results show that the intensity of diffraction peaks in XRD spectra decreases with increase of ion fluence as shown in fig.14 (a) and fig. 14(b) of set-A and set-B respectively. It is clear from inset of fig. 14(a) that set-A shows some crystalline nature even at 1×10^{14} ions/cm^2, whereas set-B is completely amorphized at 5×10^{13} ions/cm^2 as shown in inset of fig. 14(b). It is observed that the rate of amorphization is faster in set-B sample as shown in fig. 14(c). In conclusion, radiation stability of set-A samples is more than set-B because of its stoichiometry.

References

[1] R.C. Ewing, W.J. Weber, J. Lian, J. Appl. Phys. 95 (2004) 5949.
[2] K.E. Sickafus, L. Minervini, R.W. Grimes, J.A. Valdez, M. Ishimaru, F. Li, K.J. McClellan, T. Hartmann, Science 289 (2000) 748.
[3] M.K. Patel, V. Vijayakumar, S. Kailas, D.K. Avasthi, J.C. Pivin, A.K. Tyagi, J. Nucl. Mater. 380, 93(2008).
[4] R.A. Jarjis, Nuclear Instruments and Methods in Physics Research B12 (1985) 331.

5.2.3 Evolution of Defect States at ZnS:TiO_2/N-Si Heterojunction Interface Under High Energy Radiation

Prabha Sana[1], Shammi Verma[2], K. Asokan[2] and M.M. Malik[1]

[1]Department of Physics, Maulana Azad National Institute of Technology, Bhopal- 462 051
[2]Inter University Accelerator Centre, Aruna Asaf Ali Marg, New Delhi- 110 067

Present work reports the electrical transport at the interface between n-Si (100) and an over layer of ZnS:TiO_2 Quantum dots under 120 MeV Au^{9+} ions irradiation. The *in-situ* current voltage (*I-V*) and capacitance-voltage (*C-V*) characteristics, and deep level transient spectroscopy (*DLTS*) spectra (Fig. 15) have been measured on the ZnS:TiO_2/n-Si heterojunction to provide information on the interface states and the existence of deep levels in the silicon depletion region. X-ray diffraction (*XRD*) and photo luminescence (*PL*) analysis have been done in support of the above results. The *I-V* measurements (Fig. 16) show ideality factor (η) of 3.58 which deviates from the ideal value (1.0). SHI irradiation at fluence of 1×10^{12} ions/cm^2 increases the defect states at the interface which results in an increase in ideality factor (5.79) with high value of leakage current. The *C-V* result also confirms the reduction of barrier height (φ_{BH}) to 2.08 eV from the pristine sample value of 2.43 eV. Calculated dopant concentration N_D (6.5×10^8/cm^3) has also been reduced from pristine N_D (8.6×10^8/cm^3). Further fluences 3×10^{12} and 3×10^{13} ions/cm^2 show the gradual decrease in value of η, resulted by partial defect annealing process by swift heavy ion (SHI) irradiation at the interface due to electronic energy loss process. At fluence 1×10^{13} ions/cm^2, the value of φ_{BH} and N_D are increased upto 2.85 eV and 3.5×10^9 /cm^2 respectively. *DLTS* for pristine sample has been studied at different emission rate windows. Obtained results (Fig. 15) from Arrhenius plot show three dominant *DLTS* peaks $E_1(E_V+0.03$ eV), $E_2(E_V+0.12$ eV) and $E_3(E_V+0.32$ eV). These defect states are created possibly due to diffusion of Zn^{2+} and S^{2-} ions in the Si surface, also due to oxygen related self-trapped defects in Si. The *DLTS* spectra (Fig. 15) of SHI irradiated device at fluence $1x10^{13}$ ions/cm^3 shows three levels $E_1(E_V+1.0$ eV), $E_2(E_V+0.12$ eV) and $E_3(E_V+0.8$ eV). The level E_2 at $E_V+0.12$ eV remain nearly same after irradiation. While deep energy levels E_1 and E_3 are created after ion irradiation. The *PL* spectra (Fig. 17) show emission peaks 336 nm (band to band transition), 383 nm (near and edge transition), 458 nm (Zn vacancies) and 553 nm (self-trapped excitons in Si surface). After SHI irradiation the defect related peaks are blue-shifted with increased intensity and it is confirmed by enhancement of crystalline nature from *XRD*. Above study is significantly advantageous to identify the interface defects and its modification for complex heterojunctions under SHI to understand the device performance.

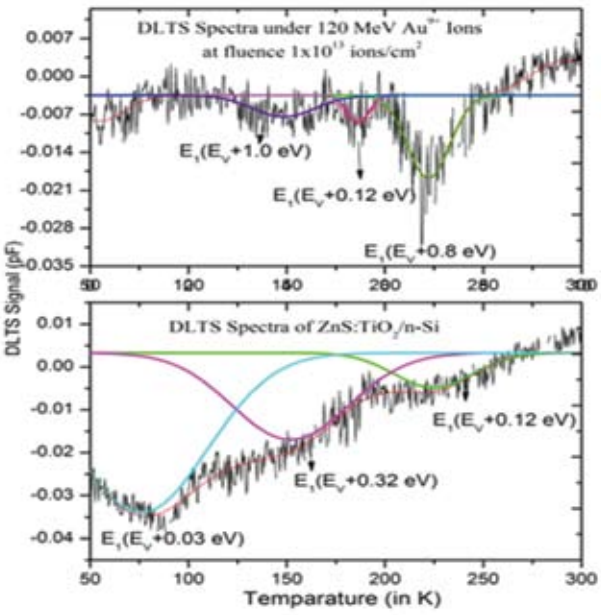

Fig. 15. DLTS spectra of pristine (bottom) and irradiated (top)

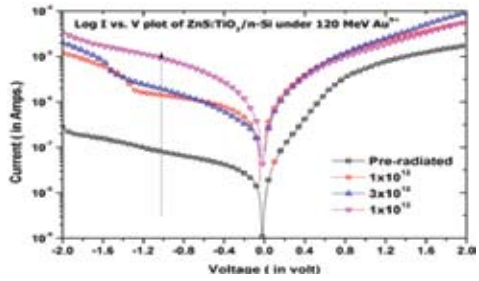

Fig. 16. I-V measurement results

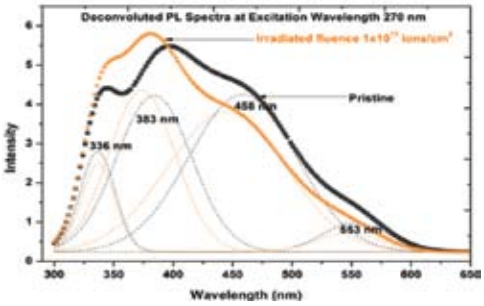

Fig. 17. Photoluminescence spectra

References

[1] P. Hazdra, D.J. Reeve, D. Sands, Appl. Phys. A 61 (1995) 637-641.

5.2.4 Synthesis of Nickel Nanostructures by Au^{9+} and Ni^{9+} Swift Heavy Ion Irradiation

Asha Attri[1], K.Asokan[2], Lekha Nair[1]

[1]Department of Physics, Jamia Millia Islamia, New Delhi
[2]Inter University Acclerator Center, Aruna Asaf Ali Marg, New Delhi

Metal nanoparticles have applications in many fields, most critically in catalysis of industrial processes [1, 2]. Motivated by the need for resources conservation and noble metal substitution in various catalytic processes, metals such as Co, Fe, Ni, Sn, have been targeted for research in nanotechnology. Nickel nanoparticles have applications in areas as diverse as carbon capture, combustion additives [3] and magnetic fluids, apart from miniaturization in the electronics industry [4].

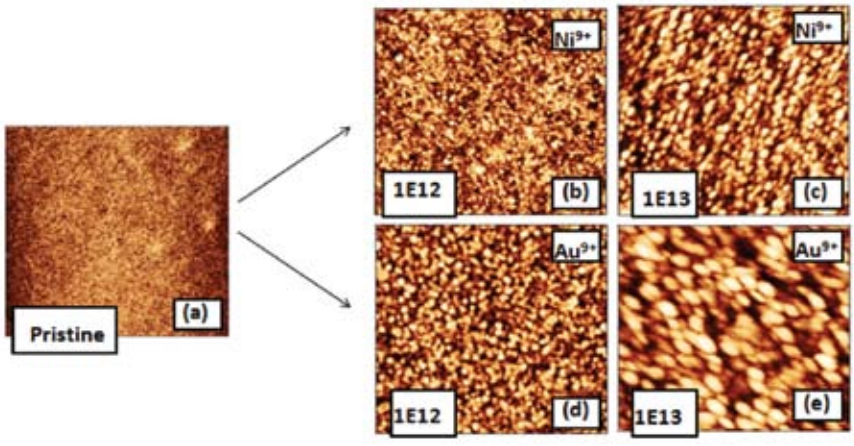

Fig. 18: AFM (1 μm ×1 μm) scans of pristine and 120 MeV Ni^{9+} and 120 MeV Au^{9+} ions irradiated samples irradiated to a fluence of 1×10^{12} ions/cm^2 and 1×10^{13} ions/cm^2.

We have synthesized Ni nanoparticles on single crystal silicon (100) substrates with swift heavy ions irradiation. 25 nm thin films deposited by e-beam evaporation were irradiated with two different ion beams i.e. 120 MeV Au^{9+} and 120 MeV Ni^{9+}, based on considerations of expected energy loss values. Transformations in surface morphology, composition and crystal structure were analyzed by AFM (Figure 18), RBS and glancing angle XRD respectively. The optimum ion energy and fluence required to generate narrow particle size distributions of Ni nanoparticles have been determined.

References

[1] Ronfang Wang, Hui Wang, Hanqing Feng, Shan Ji, Int. J. Electrochem. Sci. 8 (2013) 6068.
[2] Jitender M. K. and Kanika V., J. Chem. Sci. 124 (2012) 907.
[3] G A Bhaduri and L Šiller, Catal. Sci. Technol. 3 (2013) 1234.
[4] Xuemin He, Wei Zhong, Chak-Tong Au and Youwei Du, Nanoscale Res. Lett. 8 (2013) 446.

5.2.5 Radiation Stability of Graphene Under 150 MeV Au Ion Irradiation

Sunil Kumar, A. Tripathi, S. A. Khan, Compesh Pannu and D. K. Avasthi

Inter University Accelerator Centre, Aruna Asaf Ali Marg, New Delhi 110067, India

Due to its unique ability of reconstruction of carbon bond, graphene has a strong potential as a radiation resistant material. Atomistic simulations have demonstrated that irradiated graphene even with a high vacancy concentration, does not show any sign of instability, thus showing its applicability as robust windows [1]. Recently Recep Zan et al. [2] studied monolayer MoS_2 behaviour under electron beam irradiation and concluded that MoS_2 has high durability and lowest defect formation rate when it is encapsulated between graphene layers and suggested the radiation damage control by use of graphene. It has also been shown that encapsulation in graphene enables single particle protein complex to sustain and be imaged without damage under transmission electron microscopy (TEM) in energy range of electron used in TEM [3]. We report radiation stability of graphene under 150 MeV Au ion irradiation using Raman and XRD measurements. We observe that graphene sustains 150 MeV Au ion irradiations at high fluence without showing significant damage or amorphization. Raman measurements (fig 19a) show annealing effects at lower fluences (upto a fluence 1×10^{12} ions/cm^2) and defect production at higher fluences. XRD measurements with synchrotron (Fig 19b) show that the graphene retains significant crystallanity even at fluence of 1×10^{14} ions/cm^2. We estimated threshold fluence for complete amorphization of graphene at 2.7×10^{15} ions/cm^2 for the graphene density of 3.8×10^{15} atoms/cm^2. Our results demonstrate applicability of graphene based devices in radiation environment and space applications.

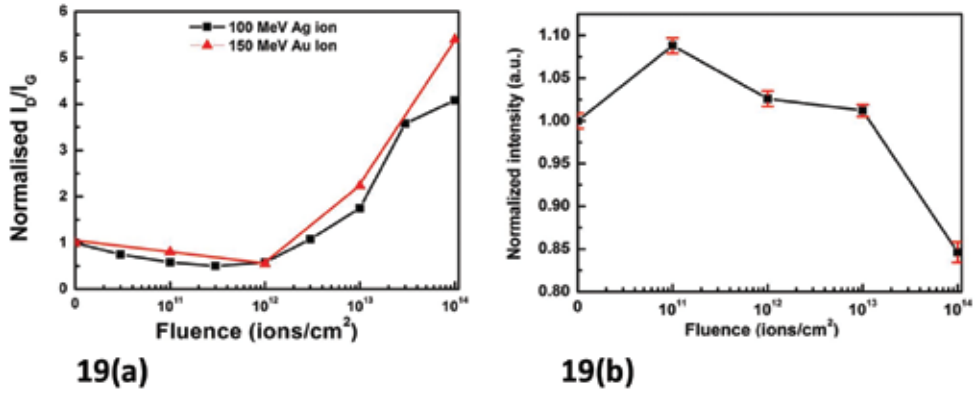

Figure 19(a) Plot of disorder parameter (I_D/I_G) with fluence for 150 MeV Au (Red curve) and 100 MeV Ag beam (black curve). 19(b) The integrated normalized graphene peak intensity with fluence from XRD measurement.

References

[1] E. H. A. Hlgren, J. Kotakski, O. Lehtinen and A. V. Krasheninnikov, Appl. Phys. Lett. 100 (2012) 233108.
[2] Recep Zan , Quentin M. Ramasse, Rashid Jalil , Thanasis Georgiou , Ursel Bangert , and Konstantin S. Novoselov, ACS Nano 7 (2013) 10167.
[3] Kasim Sader, Martyn Stopps, Lesley J. Calder, Peter B. Rosenthal Journal of Structural Biology 183 (2013) 531.

5.2.6 Volume Expansion in Crystalline and Amorphous Germanium by Swift Heavy Ion Irradiation

Sonu Hooda, S. Ojha, D. Kanjilal, D. Kabiraj

Inter-University Accelerator Centre, Aruna Asaf Ali Marg, New Delhi 110067

Single crystals of (100) oriented germanium were amorphized using 100 keV Ar ions with a fluence of 1×10^{15} ions cm^{-2}. They were subsequently irradiated by 100 MeV Ag ions. After irradiation, formation of step was observed at the boundary of irradiated and unirradiated region, indicating volume expansion due to irradiation. The increase in height of the step was also observed in 100 MeV Ag irradiated crystalline Ge (c-Ge) samples, which is compared with that of pre-amorphized irradiated samples. The step height was found to be increase with irradiation fluence in both cases. Rutherford backscattering spectroscopic channelling (RBS/C) study was carried out to correlate defects produced by irradiation and volume expansion.

Slightly n-type doped, single crystal Ge (100) was pre-amorphized using 100 keV Ar ion irradiation at a fluence of 1×10^{15} ions cm^{-2}, which corresponds to 7 displacements per atom (dpa). Further SHI irradiation was performed with 100 MeV Ag^{+8} ions at normal incidence for both a-Ge and c-Ge samples in the fluence regime of 1×10^{12}- 1×10^{14} ions cm^{-2}. At the time of irradiation half of the sample surface was covered with a sharp edge at the boundary. A Dektak stylus profilometer (with tip diameter 50 nm and height resolution of 5-10 Å) was used to measure the height difference between surface of irradiated and un-irradiated sample. Fig. 20 (a) shows the step height of pre-amorphized and crystalline Ge samples after 100 MeV Ag^{+8} ions irradiation for the fluences ranging from 5×10^{12} to 1×10^{14} ions cm^{-2}. The mean value of the step height corresponds to the volume expansion due to irradiation as shown in inset of Fig. 20 (a). It is found that in a-Ge samples the step height of ~20 nm is observed even at a fluence of 1×10^{13} ions cm^{-2}, which increases to ~84 nm at a fluence of 1×10^{14} ions cm^{-2}. The rate of increase is fast up to 3×10^{13} ions cm^{-2}, which tends to slow down after that. In case of c-semiconductor, no measurable step noticed in the samples irradiated up to 1×10^{13} ions cm^{-2}. But it increases with higher irradiation fluence. On comparing step height increase of both samples, we observe, it is more in the pre- amorphized samples up to 3×10^{13} ions cm^{-2} and they coincide in the samples irradiated at higher fluences. Using SRIM-2008 simulation the calculated value of electronic energy deposition (S_e) for 100 MeV Ag in Ge is 16.35 keV/nm, which is higher than the threshold value (10.5 keV/nm) of electronic energy loss for void formation. This indicates that the inelastic collision induced void formation in amorphous layer might have significant contribution in volume expansion of a-Ge up to a fluence of 3×10^{13} ions cm^{-2}. However, after fluence of 3×10^{13} ions cm^{-2} the voids formed at the end of the range of 100 MeV Ag is dominant for volume expansion. This indicates that pre-amorphization supports formation of voids.

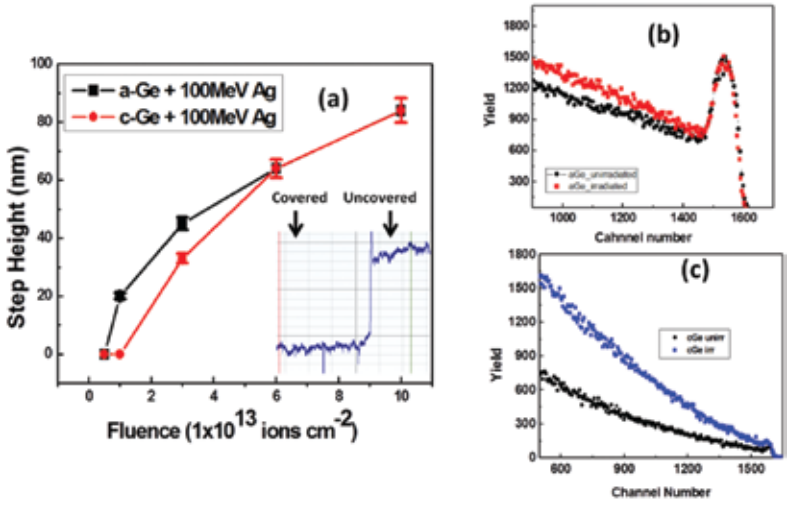

Fig.20 (a) Mean step height of the surface for a-Ge and c-Ge, irradiated with different fluences. Inset shows volume expansion in an irradiated sample as measured by surface profilometer. (b) RBS/C spectra of unirradiated and 100 MeV Ag ion irradiated a-Ge and (c) c-Ge samples to a fluence of 1×10^{14} ions cm^{-2}.

RBS/C experiments were also performed on a four axis goniometer using 2 MeV He ion beam. Fig. 20 (b) and (c) shows the RBS-C spectra of pre-amorphized-Ge and c-Ge before and after 100 MeV Ag^{+8} irradiation at a fluence of 1×10^{14} ions cm^{-2}. This shows that there is no significant change in damage of pre-amorphized-Ge as well as c-Ge, whereas, the de-channeling contribution is increased after SHI irradiation. No significant amorphization is observed on irradiating c-Ge though a step height is observed. This may be due to void formation at much deeper layers in the material.

The only difference in these two cases is the expansion in amorphous zone only, which tends to saturate at the fluence of 6×10^{13} ions cm^{-2} and no more expansion is observed on irradiation to higher fluences. It can be concluded that 200 nm of pre-amorphized zone expands by 20 nm i.e. 10 % along the direction of ion irradiation.

5.2.7 Swift Heavy Ion Induced Effect on Bimetallic Au/Fe Nanoparticles Dispersed in Silica Matrix

Compesh Pannu, Udai B. Singh, D. Kabiraj, D. K. Avasthi

Inter University Accelerator Centre, Aruna Asaf Ali Marg, New Delhi – 110067, India

Bimetallic nanostructures have different physical and chemical properties thantheir monometallic counterparts. To study this type of system is interesting in combination of two metals with different application areas. Fe based nanocomposites are magnetic in nature and Au nanocomposites have peculiar optical properties [1-2]. Au – Fe nanoparticles could combine magnetic and optical properties and offers magneto optical properties [3-4]. In the present work, we prepared Au and Fe bimetallic nanoparticles and studied swift heavy ion induced effect on these nanoparticles. In this study, Au and Fe were cosputtered along with silica for preparation of nanocomposite thin films of silca containing bimetallic nanoparticles. The thickness of the nanocomposite thin films is 450 nm and Au, Fe fraction is 19at% and 15at% respectively. These nanocomposite tihn film were irradiated with 100 MeV Au ions at varying fluences from 1×10^{13} to 6×10^{13} ions/cm^2. The structural studies of the as deposited and irradiated samples is carried at Elletra, Italy using synchrotron radiations of 15 keV energy. X ray diffraction spectra of as deposited and irradiated samples is shown in fig. 21.

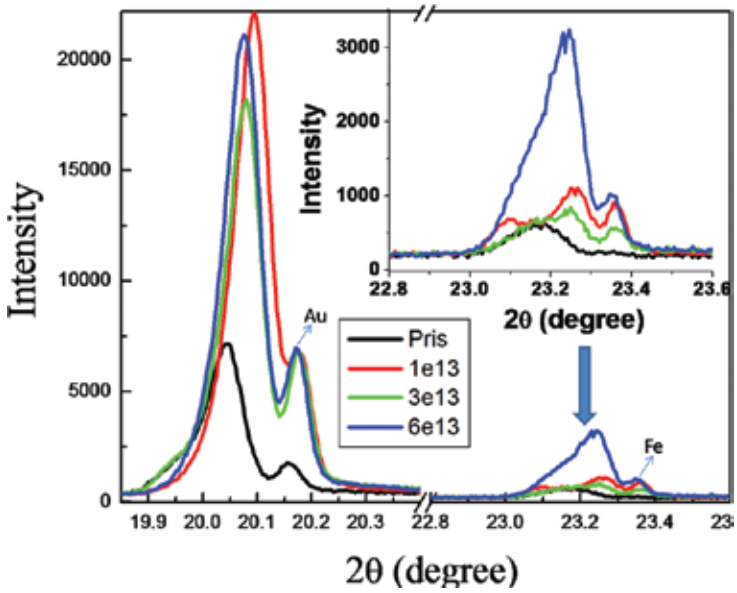

Fig. 21. X ray diffraction spectra of as deposited and irradiated samples

The peak positions of pure Au and Fe in X ray diffraction spectra using 15 keV energy are 20.22° and 23.34° respectively. In the as deposited sample, the peak centered at 20.15° is slightly shifted from pure Au peak position which indicates presence of strain. Ater irradiation this peak shifts toward the pure Au position due to release in strain. Fe in the as deposited sample may be present in the atomic form and therefore no peak corresponds to pure Fe. After irradiation, Fe (110) peak emerges due to the formation of structure between Fe atoms. The peaks centered at 20.04 and 23.17 are due to interaction between Au and

Fe resulting in to formation of Au-Fe bimetallic nanoparticles. The FWHM of both these peaks increase after irradiation which shows the decrease in grain size of bimetallic nanoparticles. After irradiation, the peak centered at 23.17° splits in to component peaks due to strong structural rearrangement leading to decomposition of bimetallic nanoparticles.

References

[1] T. Klar and M. Perner, Phys. Rev. Lett. 80 (1998) 4249.
[2] W. Rechberger and A. Ohenau, Optics Communications 220 (2003) 137.
[3] K. W. Kim and Y. H. Hyun, Phys. Status Solidi 196 (2003) 197.
[4] Y. P. Lee and Y. V. Kudrayavtsev, Phys. Rev. B 67 (2003) 104424.

5.2.8 INTERFACIAL MIXING IN Co/Sb THIN FILM SYSTEM

Manju Bala[1], S.K. Tripathi[2], K. Asokan[1], D. K. Avasthi[1]

[1]Inter-University Accelerator Centre, Aruna Asaf Ali Marg, New Delhi-110067
[2]Department of Physics, Panjab University, Chandigarh-160 014, India

In the present work, the synthesis of Co-Sb alloy using high energy heavy ion beam induced mixing of Co/Sb bilayer system is investigated, which is expected to be a good thermoelectric material [1]. The Co (~60 nm)/Sb (~100 nm) thin films were prepared by successive thermal evaporation of Co and Sb respectively over cleaned quartz substrate under the pressure 10^{-5} torr at room temperature. Mixing of bilayer was studied by (I) annealing at 380oC in the atmosphere of Ar+2%H2 for 1 hour and (II) irradiating with 100 MeV Ag^{+7} ions with beam current of 2 pnA under a varying fluence of 1×10^{14} ions/cm^2 and subsequently annealing at 380°C in the atmosphere of Ar+2%H_2 for 1 hour [2]. The pristine, annealed and irradiated samples were characterized by Rutherford backscattering spectrometry (RBS) and X-ray diffraction (XRD). The RBS spectra (Fig. 22(a)) of the pristine sample show two separate peaks for Co and Sb. It can be seen that there is a shift of Co peak towards high energy side and a reduction of yield at peak for both annealed and irradiated annealed samples. For the irradiated annealed sample, there is complete mixing of Co in Sb. To study the phase formation, XRD of the pristine, annealed and irradiated samples was done. The XRD spectra of pristine sample show peaks corresponding to Sb only which is present on the top in the bilayer system (Fig 22(b)). Annealing of the pristine sample shows peaks of Sb along with indication of CoSb, $CoSb_2$ and $CoSb_3$ phases. After irradiation at 1×10^{14} ions/cm^2 fluence and post annealing at 380°C, the Sb phase disappears completely and an additional peak appears corresponding to $CoSb_2$ only. In conclusion, annealed pristine sample shows the presence of Sb along with CoSb, $CoSb_2$ and $CoSb_3$ phases while irradiated annealed samples shows only $CoSb_2$ phase.

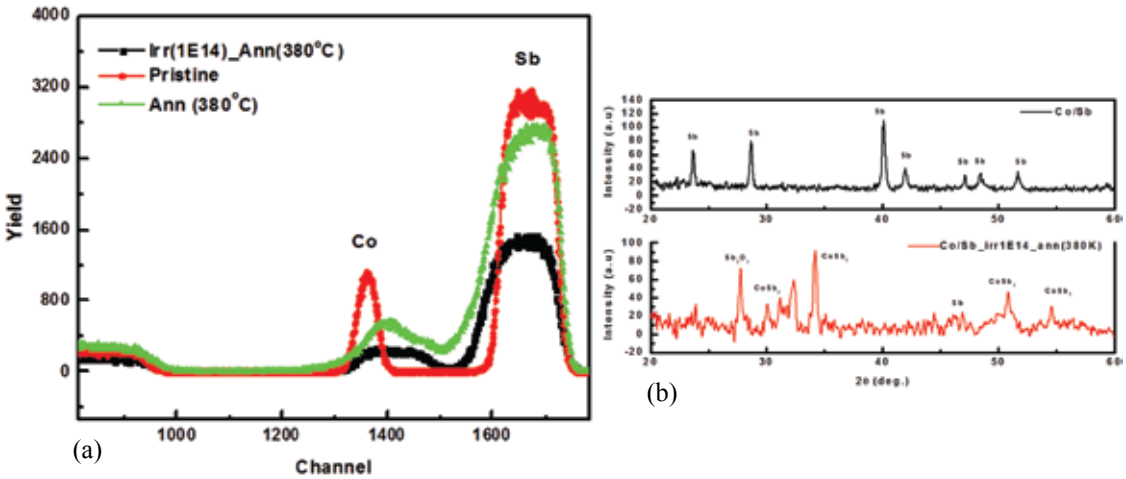

Fig. 22(a) RBS spectra of pristine, annealed and irradiated samples of Co/Sb on quartz
(b) XRD of bilayer (Co/Sb) samples pristine, annealed and irradiated annealed with 100 MeV Ag.

References

[1] Savchuk et al, Journal of Applied Physics 92 (2002) 5319.
[2] Diana et al. Adv. Mat. Lett., 5(4) (2013) 223-228.

5.2.9 140 MeV Ni Ion Irradiation Induced Structural Modifications of $AgInSe_2$

R. Panda[1], M. Panda[1], H. Rath[1], P. Dash[1], B. Dash[1], K. Asokan[2], R. Naik[1], N.C. Mishra[1]

[1] Department of Physics, Utkal University, Vani Vihar, Bhubaneswar, 751004, India
[2] Inter-University Accelerator Centre, Aruna Asaf Ali Marg, New Delhi -110067, India

The chalcopyrite silver indium diselenide is a highly important photo-voltaic material, but has not got much attention from irradiation point of view. Earlier studies [1] indicated extreme sensitivity of this system to SHI irradiation. Present study examines the evolution of the structure of this system with SHI irradiation. $AgInSe_2$ thin films were irradiated by 140 MeV Ni ions at IUAC, New Delhi. The x-ray diffraction patterns for the pristine and irradiated films at different fluences (Fig. 23(a)) indicate chalcopyrite structure with a prominent peak along the (112) at an angle (2θ) of 25.54°. The lattice parameters, a and c, of the $AgInSe_2$ sample were calculated to be 6.14Å and 11.78Å with c/a close to 2 corresponding to chalcopyrite structure. Irradiation led to increase in FWHM of the (112) peak indicating fragmentation of particles by SHI irradiation. The peak intensity decreased with increasing ion fluence and the samples were completely amorphized beyond the fluence of 1×10^{13} ions cm^{-2}. Expanded view of the (112) peak (Fig.23(b)) indicates that there is a shifting of the peak position towards right with increasing ion fluence, which indicates that 140MeV Ni ion irradiation leads to lattice compression. These results reveal that the electronic energy loss of 140 MeV Ni ions is larger than the threshold for creation of amorphized latent tracks in $AgInSe_2$ and the amorphized matter in the track region put a radial stress on the surrounding crystalline material.

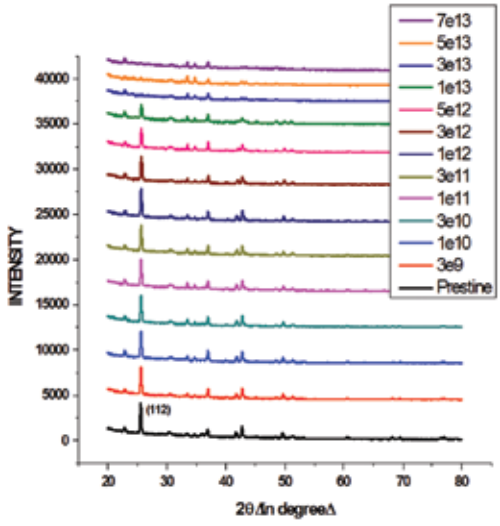

Fig. 23(a) XRD of un-irradiated and irradiated $AgInSe_2$

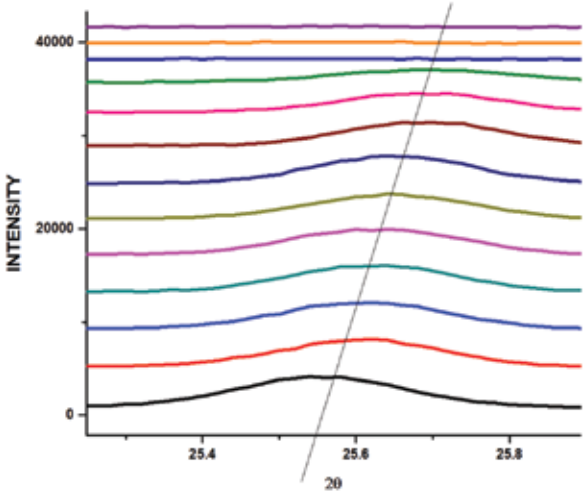

Fig. 23 (b) Shift of the peak position

References

[1] Dinesh Pathak, R. K. Bedi, Davinder Kaur, Ravi Kumar, Chalcogenide Letters Vol. 8 (2011) 213.

5.2.10 Tailoring Topographical and Magnetic Properties of Fe-Ni Alloy Based Thin Films Employing 100 MeV Ag^{8+} IONS

Lisha Raghavan[1], Hysen Thomas[2], Geetha Pookat[1], Sunil Ojha[3], Indra Sulaniya[3], D K Avasthi[3] & M R Anantharman[1]

[1] Department of Physics, Cochin University of Science and technology
[2] Christian College, Chenganur
[3] Inter University Accelerator Centre, New Delhi

Metglas 2826 having a nominal composition of $Fe_{40}Ni_{38}Mo4B_{18}$ is an outstanding amorphous soft magnetic material. Nanocrystallinity can be induced in such systems by thermal annealing and swift heavy ion irradiation. In spite of continued efforts, retaining the exact composition of bulk in the thin film form is a challenge; overcoming which can escalate the use of metglas in MEMS/NEMS devices. We have deposited the films by RF sputtering method to reproduce the target composition and study the effect of thermal annealing and SHI irradiation on $Fe_{40}Ni_{38}Mo4B_{18}$ thin films. On swift heavy ion irradiation of these films, amorphous tracks in the films are expected to be created which could alter the magnetic property and possibly result in nano patterning.

The 15UD Pelletron accelerator facility at IUAC Delhi has been utilized to carry out the experiments. Fe-Ni alloy based thin films were deposited using RF sputtering in an Ar atmosphere. 100 MeV Ag^{8+} ions were employed to modify the topographical structural and magnetic properties of Fe-Ni alloy based thin film have been irradiated to fluences of 1×10^{11}, 1×10^{12}, 1×10^{13} and 3×10^{13} ions/cm^2. The irradiated films were characterized using GXRD, AFM, SQUID VSM.

Significant surface modification resulted with irradiation which in turn paved way for modification of magnetic properties of the irradiated films. The saturation magnetisation of films increased for 1×10^{11} and 3×10^{13} irradiated films (Fig. 24). The morphological changes are evident from AFM images. (Fig. 25)

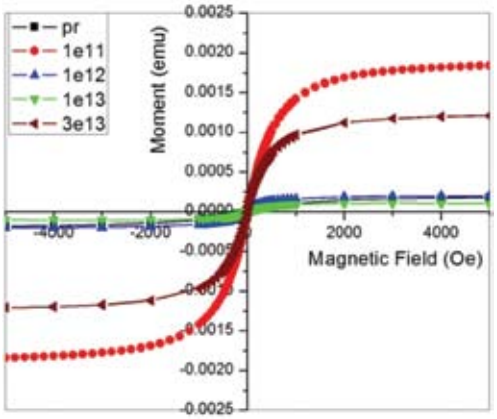

Fig. 24 Room temperature M-H curves of Fe-Ni alloy based thin films

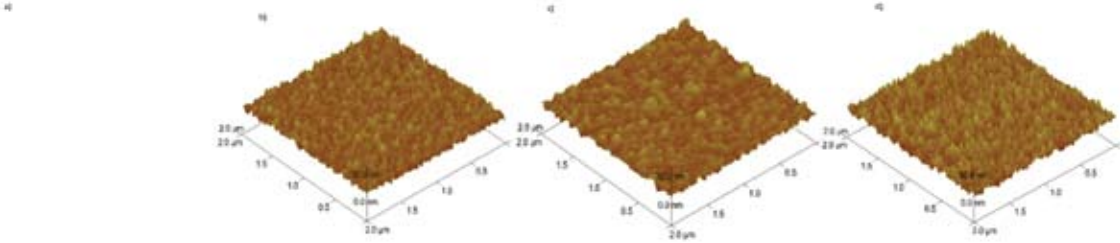

Fig. 25 AFM images of a) pristine and films irradiated to fluence of b)1×10^{12} c)1×10^{13} and d) and 3×10^{13} ions/cm^2 Fe-Ni alloy based thin films

5.2.11 Studies of Ion Beam Induced Crystallization on Metal Oxide Thin Films

Shally Bhatia and Atul Khanna

Sensors and Glass Physics Lab., Dept. of Physics, Guru Nanak Dev Univ., Amritsar, Punjab 143005, India

The effect of ion irradiation on the structural, optical, electrical and gas sensing properties of WO_3 and MoO_3 thin films was investigated. For the studies, thin films of tungsten trioxide and molybdenum trioxide were deposited on quartz, alumina and silicon substrates by thermal evaporation and characterized by XRD, UV spectrophotometer and two probe set up for electrical measurements, SEM, EDAX, Raman and AFM studies. As-deposited WO_3 films were amorphous and crystallized to monoclinic phase on annealing at 673K for 2h (Fig. 26a).The as-deposited films of MoO_3 were also amorphous and crystallized to orthorhombic phase on annealing at 623K for 1h (Fig. 26b). The band gap of WO_3 thin films decreased on annealing treatment from 3 eV to 2.4 eV. The band gap of MoO_3 thin film decreased on annealing treatment from 3.1 eV to 2 eV.

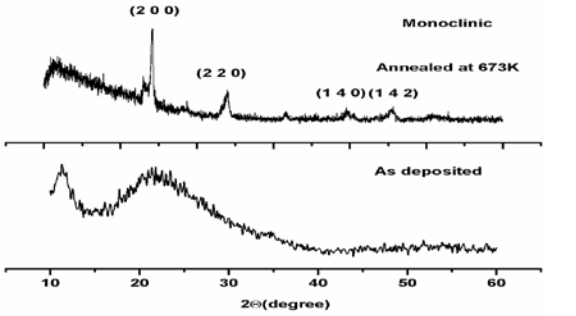

Fig.26a. XRD pattern of WO_3 thin film.

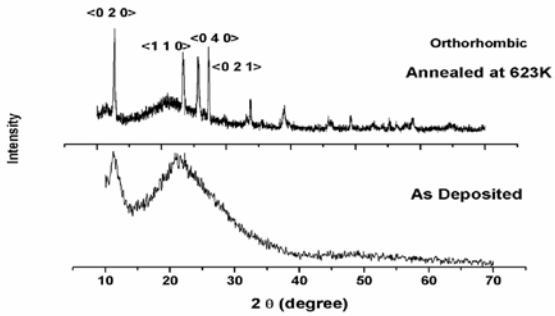

Fig.26b. XRD pattern of MoO_3 thin film.

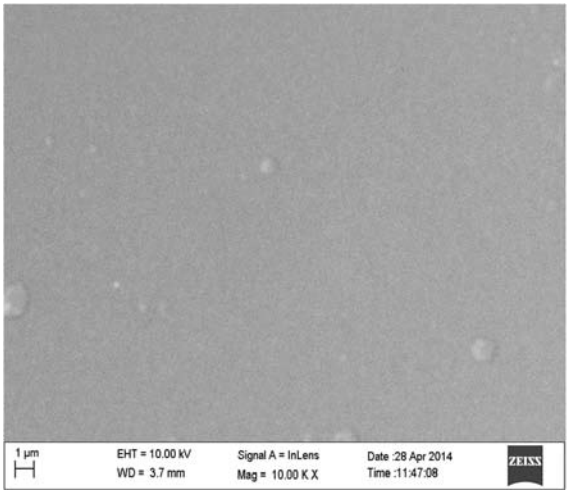

Fig. 27a. Surface morphology of amorphous MoO3 film

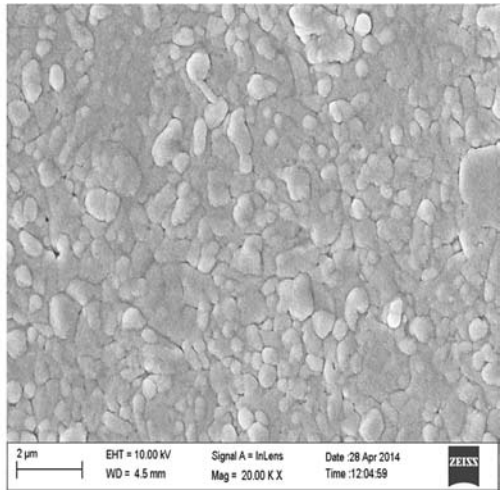

Fig.27b. Surface morphology of crystalline MoO3 film

The surface morphology of the thin film were studied by the FESEM and the FESEM images are shown in Fig.27a and 27b. The amorphous film is smooth and upon annealing it crystallizes and shows grain formation.

5.2.12 Dielectric Response of PMMA/$ZnFe_2O_4$ Composites Under 400 keVAr^{+2} Ions

Ambika Negi[1], Fouran Singh[2], R.K.Kotnala[3], D. Kanjilal[2] and S. Annapoorni[1]

[1]Department of Physics and Astrophysics, University of Delhi, Delhi-110007
[2]Inter University Accelerator Centre, Aruna Asaf Ali Marg, New Delhi - 110067, India
[3]National Physical Laboratory, New Delhi, India

Polymeric materials have a great potential in many scientific and technological applications because of their versatile properties, due to low density, ability to form intricate shapes and low manufacturing cost

[1]. The properties and applications of polymers can be modified by incorporation of filler into the polymer matrix, which leads to the formation of composite/nano-composite materials [2-3]

In the present study, PMMA films were dispersed with zinc ferrites at 50% concentrations and the possible structural and dielectric changes in the composites caused by 400 keV Ar^{2+} ion beam irradiation are studied. The XRD analysis was carried out using X-ray diffractometer (Panaylitical) with CuK_{α} radiation (λ=1.54Å) and the dielectric properties of composites were measured using Wayne Kerr 6560 LCR meter at room temperature in frequency range from 100 Hz to 120 MHz. XRD patterns of pure PMMA, pristine and irradiated PMMA+50% zinc ferrites composite films with Ar^{+2} ion beam at three different fluences 5×10^{14}, 1×10^{15} and 5×10^{15} ion/cm^2 are shown in Fig. 28. The variation in peak intensity of the composite films after irradiation shows some significant changes in the structure of the composites. The observed behavior is attributed to the cross-linking of molecular chains, which change the ordered crystallites into disordered ones by forming new bonds between the neighboring chains [4].

Fig. 29 (a) & (b) shows the dependence of dielectric constant and dielectric loss on the frequency of applied field after the irradiation. The dielectric constant remains constant up to 10 MHz and indicates that the motion of the free charge carrier is constant at these frequencies and 22. As the frequency increases beyond 10 MHz, the charge carriers migrate through the dielectric and get trapped inside the defect sites which results in the loss of dielectric constant. It has been observed that the dielectric constant also increases with the increasing ferrites contents which may be due to functionalization of ferrite to polymer enhance [5]. It is also observed that the dielectric loss decreases exponentially and then becomes almost frequency independent. This is due to induced charges which gradually fail to follow the reversing field and leads to a reduction in the electronic oscillations as the frequency is increased. 250% enhancement due to the addition of filler, which is further enhanced by 25% by irradiation. This could be understood by change in interfacial polarization mechanism of the heterogenous system.

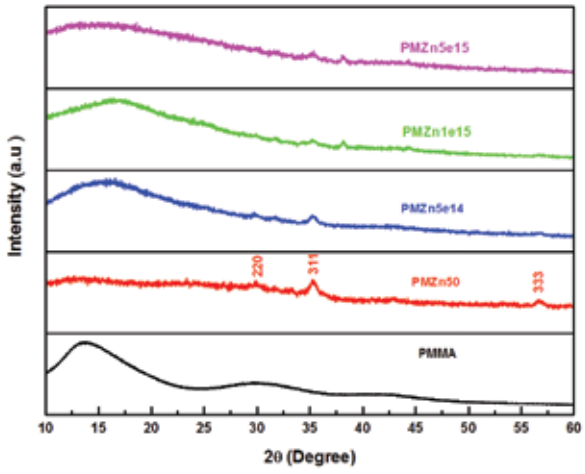

Fig.28 XRD spectra of pure PMMA , Pristine and irradiated PMMA + (50%) $ZnFe_2O_4$ at three different fluences

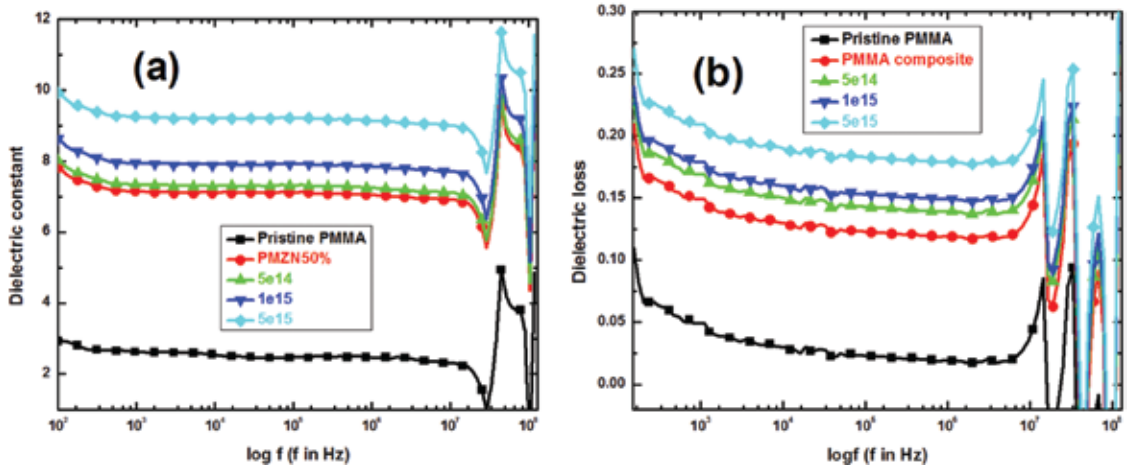

Fig. 29 (a) Dielectric constant and (b) dielectric loss of pure PMMA, Pristine and irradiated PMMA + (50%) $ZnFe_2O_4$ to three different fluences.

References

[1] Y. Wu, T. Zhang, H. Zhang, X. Xhang, Z. Deng, G. Zhou, Nucl. Instr. Meth. B 169 (2000) 89.
[2] Y. Ali, K. Sharma, V. Kumar, R. G. Sonkawade, A. S. Dhaliwal, Appl. Surf. Sci. 280 (2013) 950.
[3] Y. Ali, V. Kumar, R. G. Sonkawade, A. S. Dhaliwal, Vacuum 93 (2013) 79.
[4] Y. Ali, V. Kumar, R. G. Sonkawade, A. S. Dhaliwal, H. C. Swart, Vacuum 90 (2013) 59.
[5] Z. M. Dang, Y. H. Zhang, S. C .Tijong, Synth. Met. 146 (2004) 79.

5.2.13 Low Energy Bombardment Induced Formation of Ge Nanopatterns

Indra Sulania[1, 2], Dinesh C. Agarwal[1], Pravin Kumar[1], Kedar Mal[1], Mushahid Husain[2] and D K Avasthi[1]

[1]Inter University Accelerator Centre, Aruna Asaf Ali Marg, New Delhi 110067, India
[2]Jamia Millia Islamia, Maulana Mohammad Ali Jauhar Marg, New Delhi 110025, India

There are many ion beam parameters to form patterns such as ripples and dots on sample surface using low energy ion [1-3]. The formation of ripple patterns on Ge surface, as a function of angle of incidence of the ion beam, has been demonstrated in this report. The angle of the ion beam has been changed for θ_{ion} = 0°, 15°, 30°, 45°, 60° and 75°, keeping the other ion beam parameters same. The results have been analyzed with the help of AFM micrographs by observing the change in shape, size and roughness variation on the surface of Ge. We have used 100 keV Ar^{4+} ions at a fluence of 3×10^{17} ions/cm^2 to bombard the samples of Sb-doped Ge(100) at 300 K at a pressure of ~ $2x10^{-6}$ mbar.

The surface of the pristine Ge(100) sample has rms roughness of 0.2 nm. The surface morphology of the irradiated samples is shown fig. 30 (A-F). When we irradiated the sample at 0°, dot structures started to evolve on the surface of Ge(100) with rms roughness of 0.5 nm. The size of the nanodots was found to be ~41nm (fig. 31). At 15° incidence, the dot size increases to 52 nm and the roughness to 0.97 nm. On further increasing the angle to 30°, the alignment of the dots was observed along the direction of the beam (shown with the arrow). The rms roughness increases to 3.39 nm and size of the dots increases to 93 nm. The wavelength of the aligned pattern was observed to be 120 nm. At 45° incidence, we observed the formation of ripples with a wavelength of the aligned nanodots as ~ 128 nm and size of dots as 97 nm. The rms roughness increases to 3.67 nm. On further increasing the angle to 60°, the roughness of the samples increases to 4.32 nm.

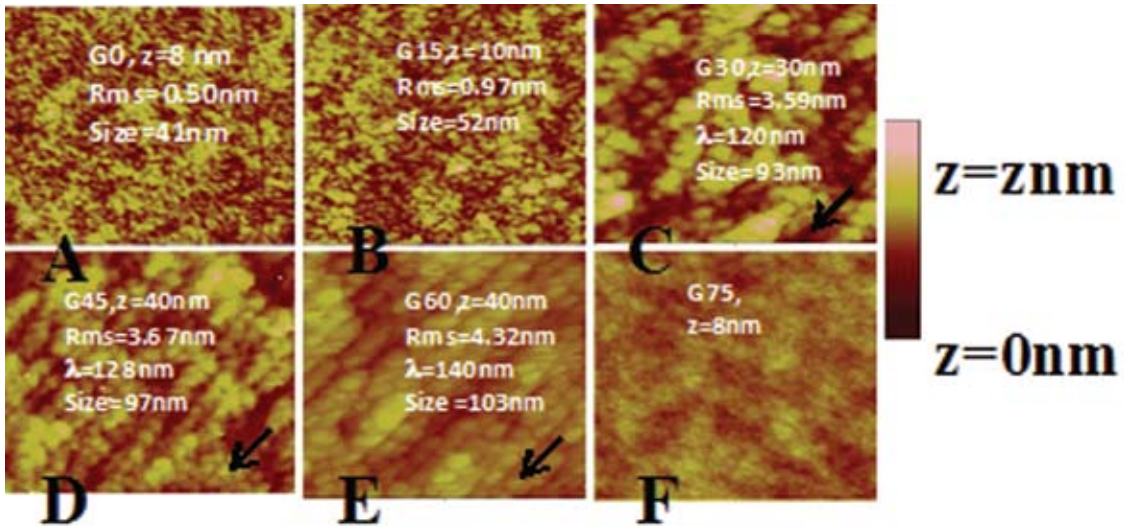

Fig. 30: AFM micrographs of the irradiated at fluence 3×10^{17} ions/cm^2 sample of Ge(100) at angle of incidence of A. 0°, B. 15°, C. 30°, D. 45°, E. 60° and F. 75°.

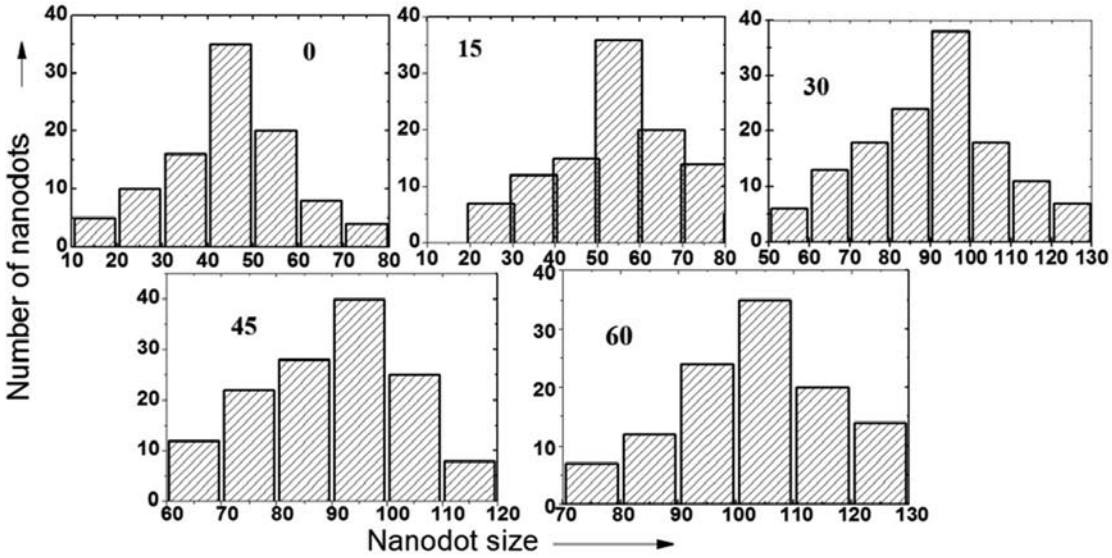

Fig. 31: Size distribution of the nanodots for different angle of incidences.

The wavelength of the ripples was found to be 140 nm and size of the dots was observed to be 103 nm. At incidence angle of 75°, the surface looks similar to the pristine sample with a roughness of 0.3 nm. At this angle, the reflection of ions takes place which decreases the probability of ions interaction with the sample surface.

Figure 32 shows the variation in rms roughness and size of dots with angle of incidence of the ion beam. The rms roughness keeps on increasing with the angle of incidence and reaches the maximum value for 60°. When the angle of incidence is changed, the ion beam is penetrating lesser; the sputtering would be more from the surface of Ge. Therefore, the roughness is maximum and the size increases to 103 nm for 60°. To conclude, the critical angle for ripple formation on Ge was found to be θ=45°.

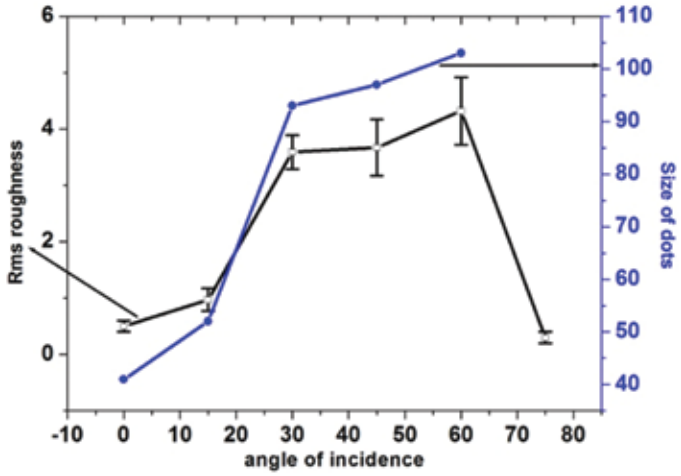

Fig. 32: Plot between angle of incidence of ion beam vs. rms roughness and size of the dots.

References

[1] F. Frost, B. Ziberi, T. Höche, B. Rauschenbach, Nucl. Instrum. Methods Phys. Res. B 16 (2004) 9.
[2] B. Ziberi, F. Frost, B. Rauschenbach, T. Hoche, Appl. Phys. Lett. 87 (2005) 033113.
[3] I. Sulania, A. Tripathi, D. Kabiraj, S. Varma, D. K. Avasthi, Journ. Nanosci. Nanotech. 8 (2008) 4163.

5.2.14 Synthesis of Embedded Au Nanostructures by Ion Irradiation of Au Thin Film on Glass

Udai B. Singh[1], D. C. Agarwal[1] , S. A. Khan[1], S. Mohapatra[2], H. Amekura[3], D. P. Datta[3,6], Ajay Kumar[4], R. K. Choudhury[4], T. K. Chan[5], Thomas Osipowicz[5], D. K. Avasthi[1]

[1]Inter-University Accelerator Centre, Aruna Asaf Ali Marg, New Delhi 110067, India
[2]Univ.School of Basic & Applied Sc., Guru Gobind Singh Indraprastha Univ., New Delhi 110078, India
[3]National Institute for Materials Science, Tsukuba, Ibaraki 305-0003, Japan

[4]Nuclear Physics Division, Bhabha Atomic Research Centre, Mumbai, India
[5]National University of Singapore, Singapore
[6]Institute of Physics, Sachivalaya Marg, Bhubaneswar 751005, India

The ion-irradiation induced synthesis of embedded Au nanoparticles (NPs) into glass from islands of Au on a glass substrate is studied in the context of recoiling atoms, sputtering and viscous flow. Cross sectional transmission electron microscopy studies revealed the formation of Au NPs embedded in the glass substrates by the 50 keV Si- ion-irradiation of irregularly shaped Au nanostructures on the glass surfaces at a fluence of 3×10^{16} ions/cm^2.

Thin films of Au with a thickness of 5 nm were deposited on these substrates by thermal evaporation with a deposition rate of 0.1 nm/s under high vacuum conditions. The vacuum of chamber before and during deposition was 2×10^{-7} and 3×10^{-6} mbar, respectively. Irradiation was performed by using 50 keV Si− ions to a fluence of 3×10^{16} ions/cm^2 at the low-energy accelerator facility (LEAF) of BARC, Mumbai. In the present case, Au NPs embedded in glass are formed due to the ion bombardment on the thin film. The Cross-sectional Transmission Electron Microscopy (XTEM) image of pristine sample is shown in Figure 33 (a). The image shows that the pristine film was discontinuous with irregularly shaped nanostructures. The glass and Au interface is shown by the dashed line. In this image traces of a few Ga NPs are observed, which originate from Ga that was incorporated during the preparation of the XTEM sample by using focused ion beam. The XTEM image [Figure 33 (b) and (c)] of the sample irradiated with a fluence of 3×10^{16} ions/cm^2 shows the presence of NPs embedded in glass. When the ions are hitting surface atoms of a nanoparticle, this primary collision generates a sudden large amount of moving target atoms by secondary knock-on events. The resulting liquid like non-equilibrium state within the nanoparticle depends on the ion beam parameters. Thermodynamic driving forces for embedding of NPs result from the different surface energies, i.e., the surface energy of the particle and its substrate, and the particle–substrate interface energy. It is reported that surface energy of embedded NPs is less than the surface energy of both glass and NPs [1]. The ion bombardment provides the critical kinetic conditions, which are responsible for the embedding of NPs. In the present studiy, the condition $EC > ER > ED$ for generating local spikes due to elastic collision cascades according to the model proposed by Bolse [2] is satisfied since E_C = 58 eV, E_R = 45 eV and E_D = 28 eV in the present case. In this way local spikes are expected to be created by ion irradiation, which may create viscous flow in the glass substrate. Thermodynamic driving forces originated from the surface and interface energies of nanoparticle and substrate are necessary to arrive at an observable ion-induced burrowing effect during ion beam irradiation because the Au nanoparticles want to minimize their surface energy. In this way embedded Au NPs can be created by ion irradiation of Au thin films, which may be an alternative way of ion beam assisted synthesis of embedded NPs after optimizing the thickness of the film and the fluence.

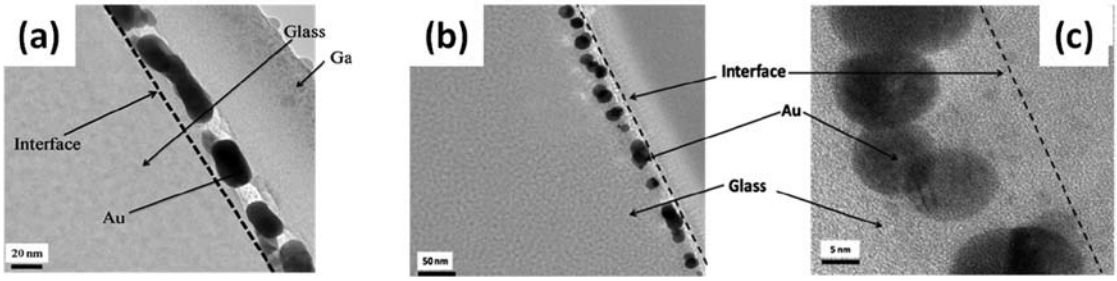

Fig. 33 (a)-Cross-sectional TEM image of the pristine sample, (b) Cross-sectional TEM image of sample irradiated with a fluence of 3×10^{16} ions/cm^2 and (c) Higher magnification XTEM image of the near-surface layer [3].

References

[1] X. Hu; D. G. Cahill,; R. S. Averback, J Appl Phys 92 (2002) 3995
[2] W. Bolse, Nucl. Instrum. Methods Phys. Res. B 80 (1993) 137-141
[3] Udai B Singh, D. C. Agarwal, S. A. Khan, S. Mohapatra, H. Amekura, D. P. Datta, Ajay Kumar, R. K. Choudhury, T. K. Chan, Thomas Osipowicz, DK Avasthi, Beilstein Journal of Nanotechnology 5 (2014) 105

5.3 RADIATION BIOLOGY RESEARCH

5.3.1 Molecular action of Moringa oleifera leaf extract and its active components on radiation protection: Assessment of low and high LET radiation effectivity.

Sanjit Dey[1], Asiti Sarma[2], Anindita Chakrborty[3] and K. Das Saha[4]

[1]Associate Professor, Department of Physiology, University of Calcutta
[2]IUAC, New Delhi
[3]UGC – DAE CSR KC
[4]IICB, Kolkata

Killing of tumour cells, using radiation therapy for the purpose of treating cancer patient has been an inevitable medical modality from its early days. Owing to its deleterious effect on normal cells or tissues during the therapy, various modulation have been made and numerous other methods are under trial in order to make this technique more safer and cost effective for the patient. One of the recent trend of research interest in the field of radiation therapy include, finding of naturally occurring compounds that can serve the purpose of radioprotectors and/or radiosensitizers with lesser side effects. In this study our main objectives were:

- To find out the modulatory role if any, of some active components of *Moringa oleifera* leaf extract namely: Quercetin, rutin and ferulic acid, upon high and low LET radiation exposure in a cell line based model.
- To evaluate the mechanism by which they complement or modulate the radiation effect in our *in vitro* study model.
- To find out the targets where we can use these compounds most effectively in order to get maximum benefits.

A. MTT cell proliferation assay:

The MTT assay is a colorimetric assay for assessing cell viability and can also be used to measure cytotoxicity (loss of viable cells) or cytostatic activity (shift from proliferative to resting status) of potential medicinal agents and toxic materials. Cells (Raw 264.7) were seeded with the density of $5x10^4$ per well of 96 wells plate (in triplicates) and incubated overnight at 37°C, 5% CO_2 and humidified atmosphere. Cells were treated with various concentrations of quercetin and incubated for different time points (1, 6 and 24 Hrs.) and finally assay was performed at 24 Hrs. OD was taken at 570nm and MTT concentration used was 5mg/ml.

B. DCFDA cellular ROS detection assay:

2', 7' –dichlorofluorescein diacetate (DCFDA) is a fluorogenic dye that measures hydroxyl, peroxyl and other ROS activity within the cell. Cells (Raw 264.7) were seeded with the density of $5x10^4$ per well of 6 wells plate (in duplicates) and incubated overnight at 37°C, 5% CO_2 and humidified atmosphere. Cells were treated with various concentrations of quercetin and NAC (10, 30, 50, 100 and 200 µM) and incubated for different time points (1 and 6 Hrs.) and finally flowcytometry assay was performed at 24 Hrs. H2DCFDA concentration used was 5µl.

C. Clonogenic assay:

A Clonogenic assay is a technique for studying the effectiveness of specific agents on the survival and proliferation of cells. It is frequently used in cancer research to determine the effect of drugs or radiation on proliferating tumor cells. HepG2 cells were used for this assay. Cells were divided into two groups: Irradiated (IR) and treated (IR+Q). Cells of both the groups were irradiated with five different doses (0.5, 1, 2, 3 and 4 Gy) of C^{6+} charged particles. Single cell suspension was made and counted in an automated

cell counter and known numbers of cells were seeded in a 75cm^2 flask and incubated in a CO_2 incubator. Similarly sham-irradiated cells were used for control experiments. Visible colonies were seen after two weeks of incubation. Colonies were stained with methylene blue and counted. Plating efficiency (PE) and Survival fraction (SF) were calculated using following formulas:

$$PE = \frac{\text{Numbers of colonies counted}}{\text{Number of cells plated}} \times 100 \quad \text{and} \quad SF = \frac{\text{PE of treated sample}}{\text{PE of control}} \times 100$$

D. Immunofluorescence assay:

HepG2 cells were grown on glass cover slips and irradiated as such. After specific time intervals cells were fixed with 1:1 methanol: acetone (ice cold) fixative solution. Using standard immunofluorescence assay technique samples were prepared and photographed in a Zeiss fluorescence microscope (AxioVision 4.7).

E. Irradiation:

Approximately 1x10^6 cells were seeded on 35mm culture plates (Nunc) and irradiated with C^{6+} ions (energy approximately 65 MeV) and γ-radiation (source ^{60}Co).

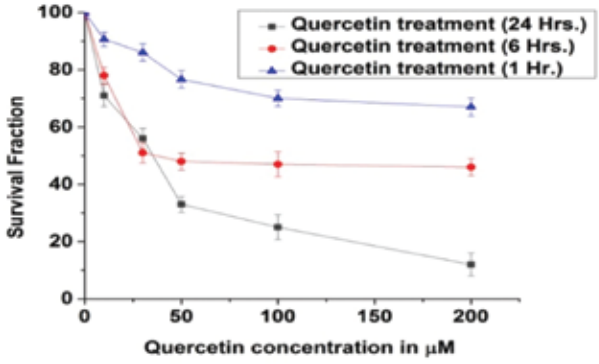

Fig.34. MTT cell cytotoxicity assay of Quercetin in Raw 264.7 cells.

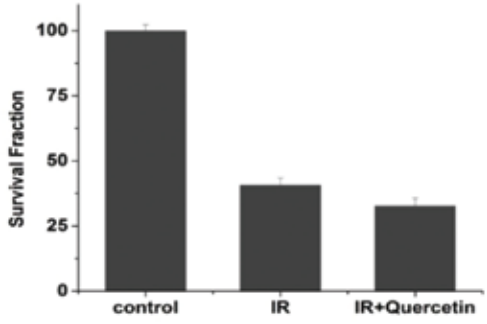

Fig.35. MTT assay of irradiated and ir+quercetin treated Raw 264.7 cells. Quercetin (30μM) treatment was carried out for 60 minutes prior to γ-irradiation.

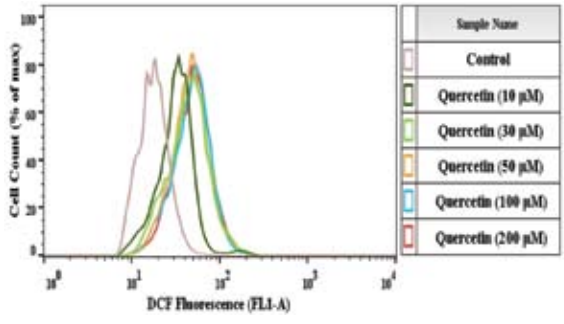

Fig.36. Flowcytometric detection of ROS via H2DCFDA staining assay in RAW 264.7 cells. Quercetin treatment was done for 60 minutes prior to H2DCFDA staining.

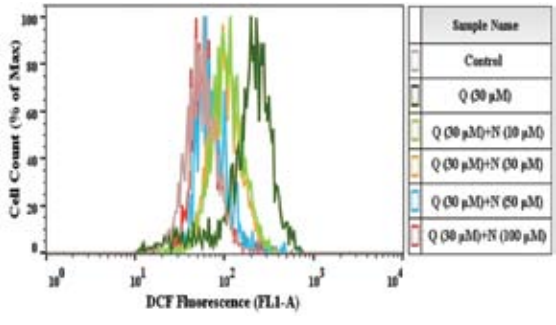

Fig.37. Flowcytometric detection of ROS via H2DCFDA staining assay in RAW 264.7 cells. Quercetin treatment was done for 1 hr. prior to H2DCFDA staining. Result depicts quercetin (30μM) induced intercellular ROS can be scavenged by an increasing concentration NAC(a potent ROS scavenger).

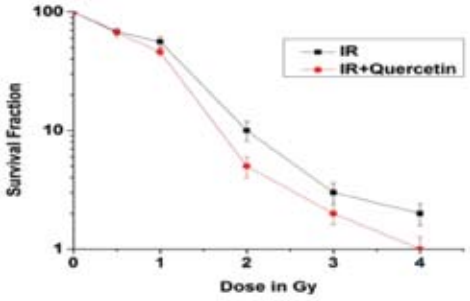

Fig. 38. Clonogenic assay of HepG2 cells upon high LET C^{6+} irradiation. Quercetin treatment was carried out 60 minutes before irradiation.

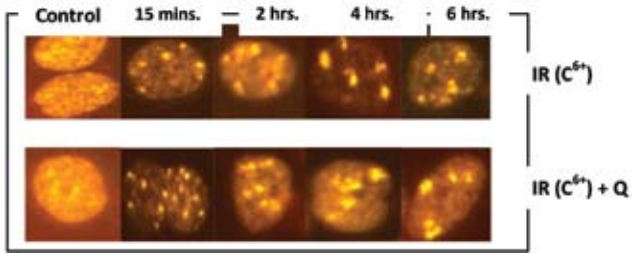

Fig.39. Formation of γH2AX foci in HepG2 cell upon high LET carbon ion radiation. Here at different time intervals after irradiation cells were fixed and sample was prepared for immunofluorescence study. A γH2AX focus indicates 1 to 1 relationship with formation of DNA DSB. During repair, the number of foci as well as the size of the foci keeps on decreasing due to dephosphorylation. Primary antibody p-ser (139) H2AX, human specific and secondary antibody conjugated with rhodamine were used.

The experimental data we have acquired so far indicating that, quercetin treatment alone renders antiproliferatic or cytotoxic effects on Raw 264.7 (Murine leukemic macrophage) and HepG2 (Human Hepato carcinoma) cells and the efficacy of these effects varies with both time and concentration dependent manner. Induction of endogenous ROS could be one of the reasons for its cytotoxic behavior towards these cell lines, at least cytometric analysis of DCFDA assay has shown this. Although cells are equipped with enzymatic as well as non-enzymatic antioxidant defense system for maintaining redox balance, uncontrollable ROS could leads to severe biological consequences, like damage to DNA and other macromolecules. As we know, repair of damaged DNA caused by high LET radiation is the most difficult task for the cellular repair apparatus, due to the complex nature of the damage, which includes: DNA; DSB, SSB and OCDL. Therefore, endogenous high level of ROS could contribute more to the high LET radiation effect. Our data of Clonogenic survival assay and immunofluorescence of γH2Ax somewhat relate our hypothesis, as we found less number of colonies and slower repair kinetics with Q+IR (^{12}C beam) group than irradiated group alone.

So far we have not checked the effects of these compounds on normal (non-cancerous) cell lines. Therefore, we are looking forward to do few experiments with normal cells. We like to find out the mechanism by which quercetin induces ROS in these cell lines. As cell cycle plays critical role in shaping the fate of a cell and also ROS can acts as a signaling molecule (concentration dependent manner) in progression of cell cycle, thus we like to find out specific cell-cycle stage where quercetin or other related compounds can put forth their effect maximally. We also like to find out the modulatory role of ROS in DNA damage and repair kinetics.

5.3.2 Targeting EGFR in A549 cells by antiEGFR antibody conjugated Au nanoparticles to achieve higher cell killing on exposure to high LET radiation

Geetanjali Pujari, Asitikantha Sarma, Devesh K Avasthi

Radiation Biology Laboratory, Inter University Accelerator Centre, New Delhi

Over expression of Epidermal Growth Factor Receptor (EGFR) in lung cancer is associated with poor prognosis of the disease. Approach is made to eliminate or reduce the expression of EGFR so as to achieve increased cell death. Targeted radiotherapy of cancer using monoclonal antibodies has been an attractive concept over the past few decades. The aim of this study is to evaluate the radio-sensitising effects of Gold nanoparticles conjugated with anti- EGFR (antiEGFR-AuNP) in lung cancer cell line A549 on exposure to carbon ion beam (^{12}C).

Colony forming assay: A549 cells were grown in 35 mm petriplates. Cells were treated with antiEGFR-

AuNP and incubated. The cells were then exposed to ^{12}C ion beam with fluence 10^6, 2X 10^6, 4x10^6, 8x10^6 and 10^7 particles/cm^2. These fluence corresponds to 0.46, 0.93, 1.9, 3.7 and 4.6 Gy. Soon after irradiation, cell survivability study was studied by colony forming assay. The irradiated cells with or without antiEGFR-AuNP were counted and 3000 cells were seeded for colony forming in 75 cm^2 tissue culture flask. Cells were incubated for 10 days till colony formation and then fixed with methylene blue. Colonies were counted and survival fraction was calculated. It is observed that treatment of A549 cells to antiEGFR-AuNP increased cell death compared to the control cells as shown in figure 40. Binding of EGFR with antiEGFR-AuNP may lead to inhibition of EGFR that in turn is unable to activate the signalling enzymes associated with cell proliferation. Also presence of Au may increase the radiosensitivity of cells due to the physical interaction of charged ions with Au (high Z element) via Compton scattering. The secondary electrons generated leads to increased radiolysis inside the cells and hence more lethal. Besides this, presence of Au may also stimulate some other enzymes associated with apoptotic and necrotic pathway that is responsible for increased cell death.

Immunofloroscence: Immunofloroscence was carried out to study the localization and expression of EGFR in A549 cells. Cells were fixed 30 minutes after irradiation and immunolabelled with monoclonal primary EGFR antibody and FITC conjugated secondary antibody. In case of the unirradiated cells, the expression of EGFR is observed in the cytoplasmic region (Figure 41).

On irradiation of A549 cells, it is observed that within 30 minutes after radiation, the EGFR expression is concentrated on the cell nucleus (figure 42). This can be explained through the role of EGFR in nuclear DNA repair process. Treatment of cells with antiEGFR-AuNP prior to radiation also showed similar trend of nuclear translocation of EGFR.

The experiment shows potential role of antiEGFR-AuNP to increase radiosensitivity in lung cancer cells. The dose reduction by approx 30% can be achieved. The analysis of EGFR expression in irradiated cells with respect to increase in dose and with antiEGFR-AuNP is to be evaluated further. Besides, investigation will also be carried out to study the enzymatic pathway dealing with cell death and DNA repair machinery.

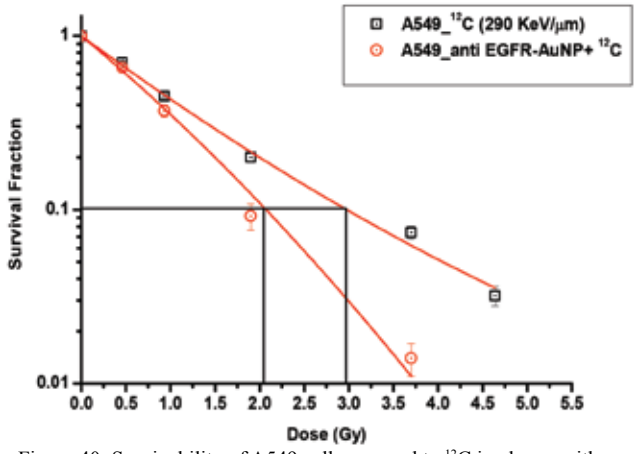

Figure 40: Survivability of A549 cells exposed to ^{12}C ion beam with or without antiEGFR-AuNP

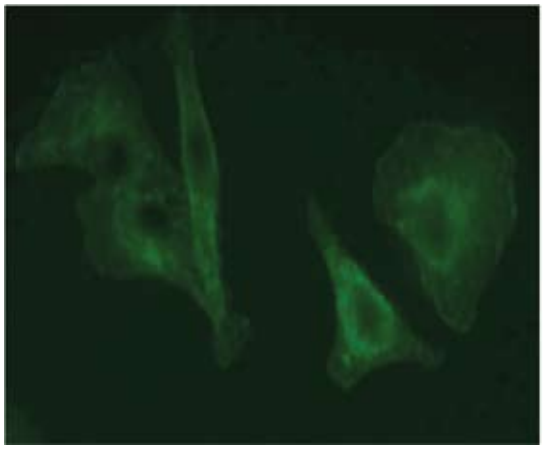

Figure 41: EGFR expression in A549 cells

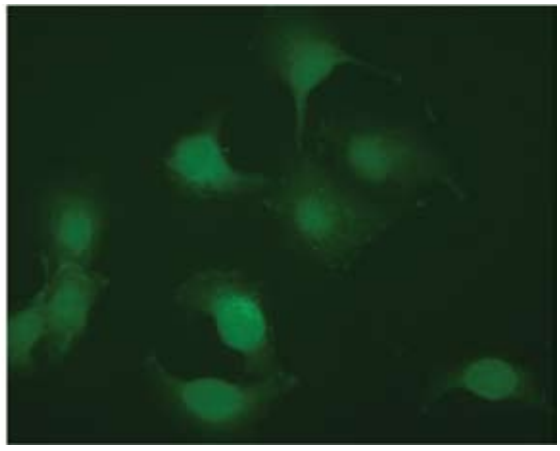

Figure 42: EGFR expression in A549 cells exposed to 1Gy of ^{12}C ion beam.

5.4 ATOMIC & MOLECULAR PHYSICS RESEARCH

5.4.1 Study of Ion-Induced Dissociation of Water Molecule

Jyoti Rajput[1] and C. P. Safvan

[1]Department of Physics and Astrophysics, University of Delhi, Delhi, India

Experiments on ion-induced dissociation of isolated H_2O molecules were conducted to study the fragmentation dynamics of this ubiquitous molecule. The powerful technique of recoil-ion-momentum-spectroscopy along with a multihit data-acquisition system was employed to extract complete information for dissociation of each single molecule. The collected data was analysed using the ROOT analysis software to identify the available fragmentation channels, to extract information about the kinematics of dissociation and to study angular correlations between the various fragments.

For complete dissociation of the molecule into three charged fragments, it was noted that intermediate molecular ions $[H_2O]^{q+}$ were formed with q as high as 5 when the fragmentation was induced using 450 keV Xe9+ ions. For the $(H^+ + H^+ + On^+)$, with 4>n>0, complete fragmentation channels, the kinetic energy of the proton increased steadily with increasing n. Protons with energy as high as 80 eV were generated during the fragmentation process.

We also found significant variations in the angular distribution of the fragment ions with respect to the incoming beam direction. Figure 43 shows such an angular distribution for the $(H^+ + H^+ + O^+)$ fragmentation channel. It is observed that the heavier fragment tend to be ejected in the backward direction with respect to the incoming beam.

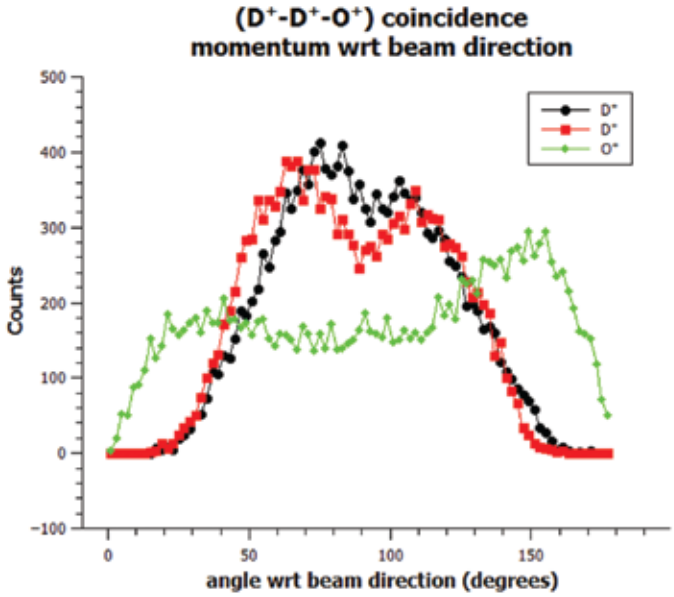

Fig. 43. Angular distribution for the $(H^+ + H^+ + O^+)$ fragmentation channel

5.4.2 Plasmon excitation in intermediate velocity proton collission with naphthalene

P M Mishra[1], J Rajput[2], C P Safvan, S Vig[1], U Kadhane[1]

[1]Indian Institute of Space Science & Technology, Trivandrum-695547, India
[2]University of Delhi, Delhi-110 007, India

Polycyclic aromatic hydrocarbons (PAHs) consist of a family of hydrocarbons containing benzene rings held together either linearly or otherwise. The structural and dynamical study for PAHs is important from astrophysical as well as biological point of view [1]. Due to delocalized electron, PAHs show collective excitation which is characterized by large oscillator strength. Due to broader energy deposition in ion-molecule collision, such excitations are difficult to isolate from other physical processes. We have distinctly identified the contribution of collective excitation in ionization and evaporation processes (H, 2H, C_2H_2

loss pathways) from the experimental results obtained from proton (50 keV to 240 keV) collision with gaseous naphthalene at Low Energy Ion Beam Facility, IUAC, New Delhi using an electron cyclotron resonance ion source [2].This study explores isolation of direct ionization and electron capture mode of collision dynamics on the basis of energetic involved in respective modes. In the direct ionization mode, two mechanisms are shown to be active in the collision process: large impact parameter plasmon excitation mode, and closer encounters with higher amount of electronic energy loss leading to fragmentation, whereas the resonant electron capture process was found to be associated with less electronic energy loss.

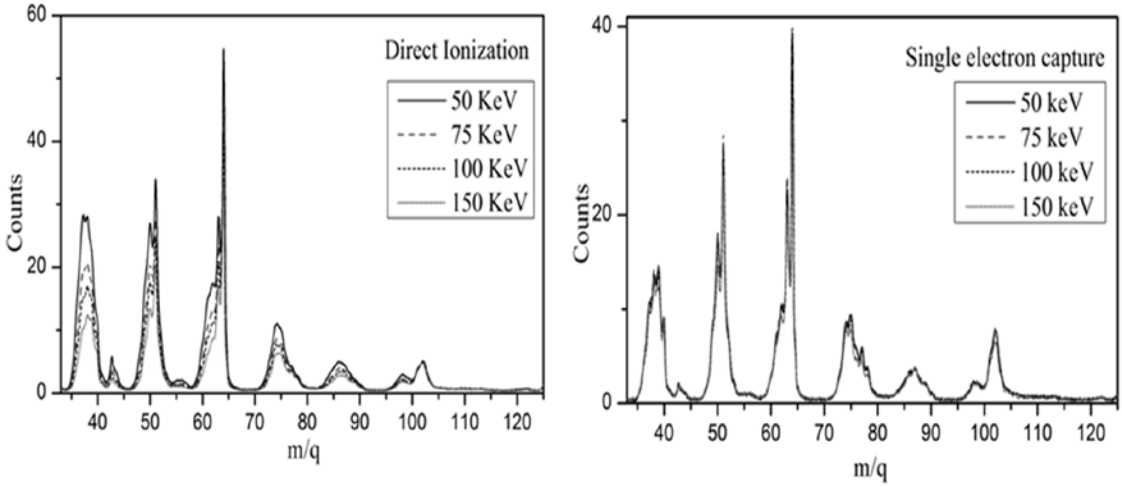

Fig. 44: Mass spectra normalized to parent single ionization peak area for different proton projectile energies.

References

[1] A. G. G. M. Tielens, Annu Rev. Astrophys. 46, 289 (2008)
[2] P. M. Mishra, J. Rajput, C. P. Safvan, S. Vig, U. Kadhane, Phys. Rev. A 88, 052707 (2013)

5.4.3 An unusual Electron Capture Phenomena by Bare Ions produced in Nuclear Reactions

T. Nandi and Prashant Sharma

Inter-University Accelerator Centre, JNU New Campus, New Delhi 110067

X-ray lines of H-like ions belonging to the projectile like fragments were observed during beam-foil experiments with ion energy exceeding the Coulomb barriers [1] [2] [3]. It was a big surprise that charge state of projectile like fragment ions were higher than that of projectile ions. In order to reveal that the source of the H-like ions is of nuclear origin, we have carried out several experiments in our laboratory. Every experiment indicated that the α-transfer reaction was a major channel. This fact is quite evident with the carbon target as ${}^{12}_{6}C$ is predominantly a 3-α cluster nuclide. Having an α-particle picked up by the projectile ion from the ${}^{12}_{6}C$, the remaining ${}^{8}_{4}C$ will decay into two α-particles almost instantly because of its short half life of 6.7×10^{-17}sec. As a result one has to detect two α-particles simultaneously in an experiment. Subsequently, two alpha particles were measured in coincidence using ${}^{56}_{26}Fe\,({}^{12}_{6}C,\ {}^{8}_{4}Be)\,{}^{60}_{28}Ni$ and ${}^{58}_{28}Ni\,({}^{12}_{6}C,\ {}^{8}_{4}Be)\,{}^{62}_{30}Zn$ reactions [4]. This time X-rays emitted at t=0 were recorded at different beam energies above the Coulomb barrier and Ly-α as well as Ly-β transitions in H-like ions were observed with the target like fragments as shown in Fig. 45.

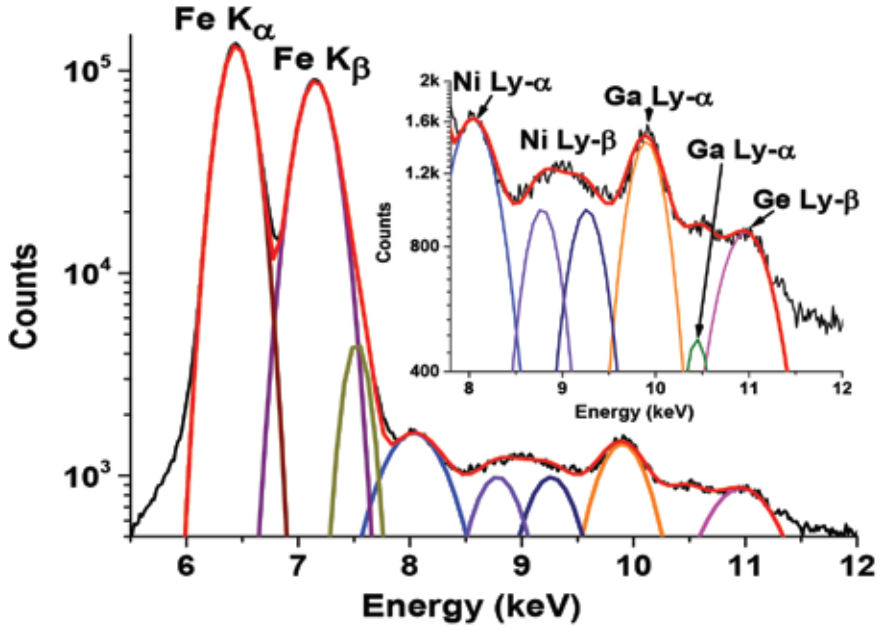

Fig 45: X-ray spectrum of the nuclear reaction for ${}^{56}_{26}Fe\,({}^{12}_{6}C,\ {}^{8}_{4}Be)\,{}^{60}_{28}Ni$ at 60 MeV

Calibration of X-ray spectra were confirmed by internal calibration using Fe K_α and K_β lines. In order to understand the origin of these X-ray lines we propose a model here that in the first instance nuclear reactions create fully stripped target-like ions that capture electrons from pseudo target atoms in excited states and emanate corresponding X-rays. Here pseudo target atom implies that target atom without its nucleus as produced just at the point of time when α is transferred from projectile to target atom as shown in Fig. 46.

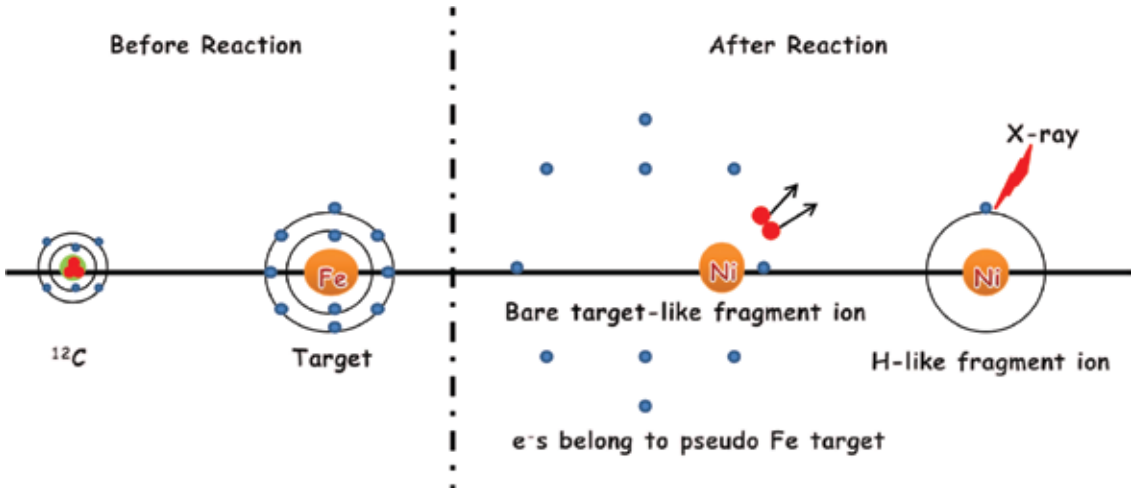

Fig 46: Schematic of the model explaining an entirely new electron capture process

We found that electron capture cross-section is quite large which makes X-ray line intensity of H-like fragment ions much more intense than one usually expects. For example, the ratio of K-shell ionization cross section and σ_{trans}-transfer cross section is of order of 10^{-6}, however, the ratio of K-shell ionization cross section and Ly-α production cross section is found to be in the order of 10^{-4}. This is the effect of large electron capture cross section that is determined from the following equations:-

$$Y_{K\alpha}^{At.} = \sigma_{K\alpha} N_P N_T \Omega \varepsilon \quad \text{.....(1)}$$

$$Y_{Ly-\alpha}^{Nucl.} = (\sigma_{trans} N_P N_T) N_T \Omega \varepsilon \sigma_{cap}^{2p} \quad \text{.....(2)}$$

$$\frac{Y_{K\alpha}^{At.}}{Y_{Ly-\alpha}^{Nucl.}} = \frac{\sigma_{K\alpha}}{\sigma_{trans} N_T \sigma_{cap}^{2p}} \quad \text{.....(3)}$$

where,

$Y_{K\alpha}^{At.}$ = Atomic yield i.e. measured Kα X-ray yield due to ^{12}C impacting on ^{56}Fe target

$Y_{Ly-\alpha}^{Nucl.}$ = Nuclear yield i.e. measured Ly-α X-ray intensity of target-like fragment ions; in this case H-like ^{60}Ni

$\sigma_{K\alpha}$ = K-shell ionization cross section determined using an atomic code [5]

σ_{trans} = α transfer cross section as measured by us [4]

N_T = Number of target atoms = 2.6×10^{18}

N_P = Number of projectile ions falling on the target per second

σ_{cap}^{2p} = Cross-section for single electron capture to 2p shell of the bare target-like fragment ions that to be determined from the above equation (3).

To quote representative result: σ_{cap}^{2p} for 60 MeV ^{12}C on 170 µg/cm^2 thick ^{56}Fe=8.0E-17cm^{-2}. In the next phase, several experiments were conducted in the inverse kinematic condition emulating the beam-foil spectroscopy experiments at different beam energies below and above the Coulomb barrier. The observed X-ray spectra show even more surprise when one notices the intensity ratios between the X-ray line intensity of the projectile ions and that of the projectile-like fragment ions in the order of 10. This scenario is also explained with similar model. In this case, the projectiles like fully stripped ions capture electrons from the target of pseudo projectile ions.

References

[1] N. Ahmad, R. K. Karn, P. Marketos, and T. Nandi, Nucl. Instruments Methods Phys. Res. Sect. B Beam Interact. with Mater. Atoms 233, 191 (2005).

[2] T. Nandi, J. Phys. B At. Mol. Opt. Phys. 42, 125201 (2009).

[3] A. P. Mishra, T. Nandi, and B. N. Jagatap, J. Quant. Spectrosc. Radiat. Transf. 118, 70 (2013).

[4] B. J. Roy, A. Parmar, T. Nandi, B. Mohanty, M. Oswal, A. Jhingan, V. Jha, and D. Biswas, EPJ A 58 (2014).

[5] Ž. Šmit, Nucl. Instruments Methods Phys. Res. Sect. B Beam Interact. with Mater. Atoms 36, 254 (1989).

5.5 ACCELERATOR MASS SPECTROMETRY RESEARCH

5.5.1 Distribution of atmospheric ^{10}Be in the surface sediments of Sambhar Lake, Rajasthan

Shail V. Ekka[1], J. K. Pattanaik[1], Premchand Kisku[1], Rajveer Sharma[2], Pankaj Kumar[2], S.Chopra[2]

[1]Indian Institute of Science Education and Research Kolkata, Mohanpur, WB
[2]Inter-University Accelerator Centre (IUAC), New Delhi- India

Atmospheric ^{10}Be has proved to be a potential tracer to find out sedimentation rate, paleoclimatic variation, past solar activities etc. ^{10}Be is produced in the atmosphere by spallation reaction when the cosmic ray interacts with the nuclides of oxygen and nitrogen. As ^{10}Be is highly particle reactive it binds to the aerosols and is subsequently deposited in natural archives as wet and dry deposits. ^{10}Be can be present in different phases such as exchangeable, organic, carbonate and residual of lake sediments.

Objective of this study is to observe the distribution of ^{10}Be in the Sambhar lake sediments. For this study, surface sediment samples were collected using 5cm PVC pipe from different parts of Sambhar Lake and were further sub-sampled at 1 cm interval. The top layer from 0-1cm was marked as SL-1-1, second layer from 1-2cm was marked as SL-2-1 and so on. About one gram of dried powder samples was taken for the ^{10}Be study. Beryllium was pre-concentrated from water soluble and acid soluble (8 N HCl +H_2O_2 at room temperature) phases of the sediment separately using ion exchange column chromatography. Finally $Be(OH)_2$ precipitates were converted to BeO by step heating up to 900º C in a quartz vial. It was later mixed with Nb powder and used for ^{10}Be/^{9}Be ratio measurement in the AMS facility of IUAC, New Delhi. The bulk mineralogical analysis of the surface sediments were also carried out using powder XRD.

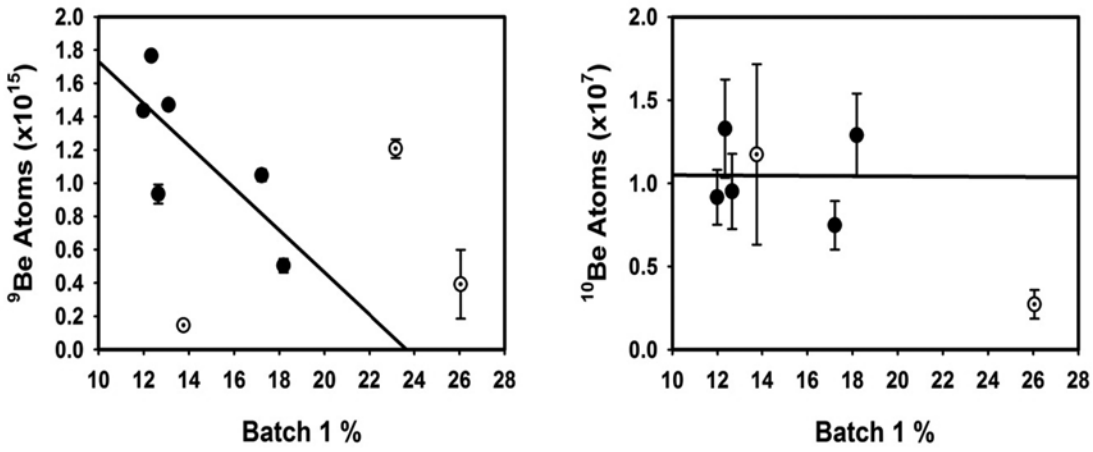

Fig. 47: Correlation of the percentage of water soluble phase (Batch 1) of the sediment with ^{9}Be and ^{10}Be concentration. The regression lines are plotted only for the samples plotted as filled circle.

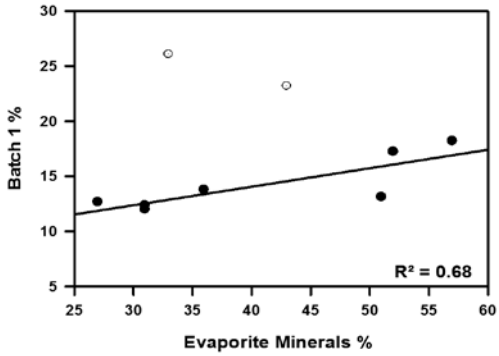

Fig. 48: The percentage of water soluble phase of the sediment is positively correlated with the percentage of evaporite mineral present in the sediments. The regression lines are plotted only for the samples plotted as filled circle.

The observed ^{10}Be concentration in the water soluble phase (Batch 1) of the sediments is varying between 0.27 ± 0.08 to $1.29 \pm 0.29 \times 10^7$ atoms/g. Whereas, in the acid soluble phase (Batch 2), ^{10}Be concentration is higher and ranges from 5.73 ± 0.93 to $16.60 \pm 1.92 \times 10^7$ atoms/g. The results indicate that the 90±6% of atmospheric ^{10}Be present in the acid soluble phase of the sediments. The percentage of water soluble phase of the sediment does not correlate with the ^{10}Be concentration but ^{9}Be shows a negative correlation (Fig. 47). The percentage of water soluble phase of the sediment is positively correlated with the percentage of evaporite mineral present in the sediments (Fig. 48). As the Sambhar is a hypersaline lake, evaporite minerals are common in the surface sediment. But the atmospheric ^{10}Be as well as ^{9}Be mainly derived from the catchment area of the lake does not get incorporated in the water soluble phase of the evaporite minerals. Since 'Be' is particle reactive element, it does not stay in the water column longer duration and gets removed quickly after entering into the lake, thus its concentration is high in the acid soluble phase. The acid soluble phase includes carbonate, oxides and organic phase of the sediments. As only 10% of the total atmospheric ^{10}Be is staying in the water soluble phase, the redistribution of ^{10}Be in the sediment column during monsoon and summer is minimal. Hence, atmospheric ^{10}Be from acid soluble phase can be used in the lake sediment for estimation of sedimentation rate and the flux. This work is in progress to better understand the distribution of ^{10}Be in the lake sediments.

5.5.2 Burial dating of artifact samples from Tikoda, Madhya Pradesh using Accelerator Mass Spectrometer (AMS)

Soumya Prakash Dhal[1], S. Balakrishnan[1], S. B. Ota[2], Pankaj Kumar[3], S.Chopra[3]

[1]Dept. of Earth Sciences, Pondicherry University, India, 605014
[2]Archeological Survey of India, Central Zone, Bhopal, India, 462003
[3]AMS Group, Inter-University Accelerator Centre, New Delhi-110067

South Asia is rich in Acheulian sites which have been attributed to the middle Pleistocene on the basis of a small number of dates. Evidences from Africa suggest that it emerged around 1.6 Ma ago and limited evidences suggest that Acheulian hominins appeared in India much later than in Africa or south-west Asia. But recent a work (Shanti, P. et al., 2011) shows that the hominins appeared in India contemporary to some other Acheulian sites and Acheulian in India is older than previously thought.

To understand the period of Acheulian technology in India we need to measure the burial dates of artifacts. (Artifacts are the stone tools prepared and used by the earlier humans for cutting and hunting purposes). With the collaboration of Archeological Survey of India (ASI) we collected several artifacts (flakes, cleavers, cores etc.) from Tikoda, Raisen District, Madhya Pradesh (Fig. 49). Samples are grinded to fine powder and quartz was separated by magnetic separation and heavy liquid separation method. Separated quartz samples were digested and passed through anion and cation columns to collect Be and Al fractions. Two different cosmogenic nuclides are needed to determine burial ages for which exposure ages also need to be determined. First, it is unknown how long the sample was exposed prior to burial and second, it is also unknown how long the sample has been buried. The concentrations of two different cosmogenic nuclides in the same clast provide enough information to solve for the above two unknowns (Granger and Muzikar, 2001). As quartzite rock bears the target nuclide of both ^{10}Be and ^{26}Al that decay with different rates we choose these nuclides to solve the problem.

Fig 49: Artifacts collected from Tikoda, Raisen District, Madhya Pradesh

For testing the methodology, four samples have been analysed for ^{10}Be using Accelerator Mass Spectrometer (AMS) at IUAC, New Delhi, which show promising results. The chemical processing for other samples is in progress in Department of Earth Sciences, Pondicherry University and measurement of ^{26}Al and ^{10}Be in remaining samples will be carried out shortly.

References

[1] Shanti P., et al., 2011, " Early Pleistocene presence of acheulian hominins in South India", Science, vol- 331, 1596-1599
[2] Granger and Muzikar, 2001, "Dating sediment burial with in situ-produced cosmogenic nuclides: theory, techniques, and limitations", EPSL, 188, 269-281.

5.5.3 An environmental magnetic study and elemental composition of a marine sediment core from the central western Bay of Bengal: implications for paleo-oceanographic studies

P.V.L.narayana[1], Pankaj Kumar[2], Archna Bohra[2], Rajveer sharma[2], Soumya Prakash Dhal[3], S.Chopra[2], I.N.Rao[4] and A.D.P.Rao[1]

[1]Department of Nuclear Physics, Andhra University, Visakhapatnam, Andhra Pradesh-530 003
[2]Inter-University Accelerator Centre, Aruna Asaf Ali Marg, 110067, New Delhi
[3]Department of Physics, Pondicherry University, Pondicherry – 605014, India
[4]Marine Chemistry Division, School of Chemistry Andhra University, Visakhapatnam, Andhra Pradesh-530 003

The Gravity Core of 4.17m length was collected during the 157th cruise of O. R. V. Sagar Kanya (October 2000) from the marginal coastal waters of central western Bay of Bengal, covering the continental shelf off Krishna Delta (Nizampatnam Bay). The elemental analysis was carried out by using PIXE experiments and the dating of the core was carried out at IUAC using AMS facility [1].

Major elements like Iron (Fe), Calcium (Ca), Potassium (K), Titanium (Ti) and Manganese (Mn) and trace elements like Vanadium (V), Chromium (Cr), Nickel (Ni), Copper (Cu), Strontium (Sr), Rubidium (Rb), Zinc (Zn) and Scandium (Sc) were also determined in the present core sediment samples using PIXE technique. The enrichment of trace metals in the core shows in the order of Cr > Sr > V > Zn > Rb > Ni > Cu > Co > Sc.

Dating studies of the core sediments are useful to delineate possible Holocene/Pleistocene boundary. The details of the dating, rate of sedimentation and their interpretation are given in Table.1. Seven sections of core samples i.e., from 50 to 350 cm having 50 cm intervals (7 samples) were dated by determining cosmogenic radionuclide ^{10}Be concentration present in the sediment samples.

Depth (cm)	Age (year)	Sedimentation rate (cm/year)
50	1300±169	0.013
100	4902±637	0.008
150	11120±1446	0.006
200	19879±2584	0.004
250	31212±4958	0.004
300	45161±5871	0.003
350	61786±8032	0.006

The rate of sedimentation in the upper part (0 – 150 cm) of this core is 9 cm/kyr, while the rate of sedimentation in the range 150 – 350 cm of the core is 4.25 cm/kyr. The total rate of sedimentation in the entire core up to 350 cm is 6.2 cm/kyr. In the core, obtained low sedimentation rate at depth 300 cm is 3cm/kyr belong to the Pleistocene period and high rate of sedimentation at depth 50 cm is 13 cm/kyr which belongs to Holocene period. Based on the ages and rate of sedimentation of the present core, the depth range from 0 to 150 cm belongs to Holocene period and after 150 cm it considered to be the Middle Pleistocene period. This is also corroborated by the obtained data of $CaCO_3$ and magnetic susceptibility. Similar age and sedimentation rates of the core from the continental margin of the south western Bay of Bengal was reported by Sri Rama Krishna et.al [2] and in the Nizampatnam Bay by Venkateswara Rao et.al [3]. Magnetic susceptibility studies were also carried out on the whole core.

Based on the ages and rate of sedimentation of the present core, the depth range from 0 to 150 cm belongs to Holocene period and after 150 cm it considered to be the Middle Pleistocene period. This is also corroborated by the obtained data of CaCO3 and magnetic susceptibility.

References

[1] Pankaj Kumar., Pattanaik, J.K., Ojha, S., Gargari, S., Joshi, R., Roonwal, G.S., Balakrishnan, S., Chopra, S., Kanjilal, D., 2011. J. Raad Nucl Chem DOI 10.1007/s10967-011-1184-x.

[2] Sri Ramakrishna, M., 2006. A Study of some stratigraphic tool for the Indian Ocean sediments. Ph.D Thesis, Andhra University, Visakhapatnam (unpublished).

[3] Venkateswara Rao, M., 2008. Textural, geochemical and palynological studies of sediment cores from Bay of Benagal, India. Ph.D Thesis, Andhra University, Visakhapatnam (unpublished).

5.5.4 ^{10}Be in the Sediments from the Krossfjorden and Kongfjorden Fjord System, Svalbard, Arctic Ocean: Paleoclimatic implications

Pankaj Kumar[1], J.K. Pattanaik[2], N. Khare[3], S. Chopra[1], Sudesh Yadav[4], S. Balakrishnan[5] and D. Kanjilal[1]

[1]Inter-University Accelerator Centre, New Delhi
[2]Department of Earth Sciences, IISER Kolkata
[3]Ministry of Earth Sciences, Prithvi Bhavan, Lodhi Road, New Delhi
[4]School of Environmental Sciences, Jawaharlal Nehru University, New Delhi
[5]Department of Earth Sciences, Pondicherry University, Pondicherry

Global warming in the recent years has been main factor of retreat of many high latitude glaciers. Fjord systems in the polar region are the most suitable sites to understand the seafloor modification, sediment supply to the marginal environment and other features related to glacier movement. Cosmogenic ^{10}Be in combination with grain size, major elemental concentration of deposited sediment can be used to understand the climatic variation in past. The Krossfjorden and Kongsfjorden system (Fig. 50) is a suitable site for understanding the glacial history and paleoclimate. Svalbard glaciers have retreated in the recent years [1, 2] and it is expected that it might have supplied more terrigenous material and melt water to these fjord systems. Here, an attempt is made to observe the accumulation and dispersal pattern of ^{10}Be in west coast of Svalbard, where two fjord systems (Krossfjorden and Kongfjorden) shares a combine mouth.

^{10}Be concentration in sediments varies between 0.90×10^8 to 2.53×10^8 atoms/g, whereas, ^{9}Be varies from 5.5×10^{16} to 11.5×10^{16} atoms/g. These sediments are mainly composed of silt (4 - 63 μm) and clay (0-4 μm) size particle and the ratio of clay/silt varies from 0.2 to 0.6. Concentration of MgO, CaO, SiO_2 and Al_2O_3 vary among the sediment samples.

Results show atmospheric input is the dominant source of ^{10}Be in sediments from the region studied. The concentration of ^{10}Be in sediments mainly depends on amount of melt water coming to fjord systems.

Calculated ^{10}Be accumulation rate varies from 3.1×10^6 atoms/cm^2/y to 8.6×10^6 atoms/cm^2/y which is higher than the accumulation rate observed in the deep sea sediment core of Arctic Ocean and Norwegian

Sea. High atmospheric ^{10}Be accumulation can be interpreted as, atmospheric produced ^{10}Be trapped in the glaciers over a period of time, is coming to the sediments due to higher outflow of melt water from the Svalbard glacier to the basin.

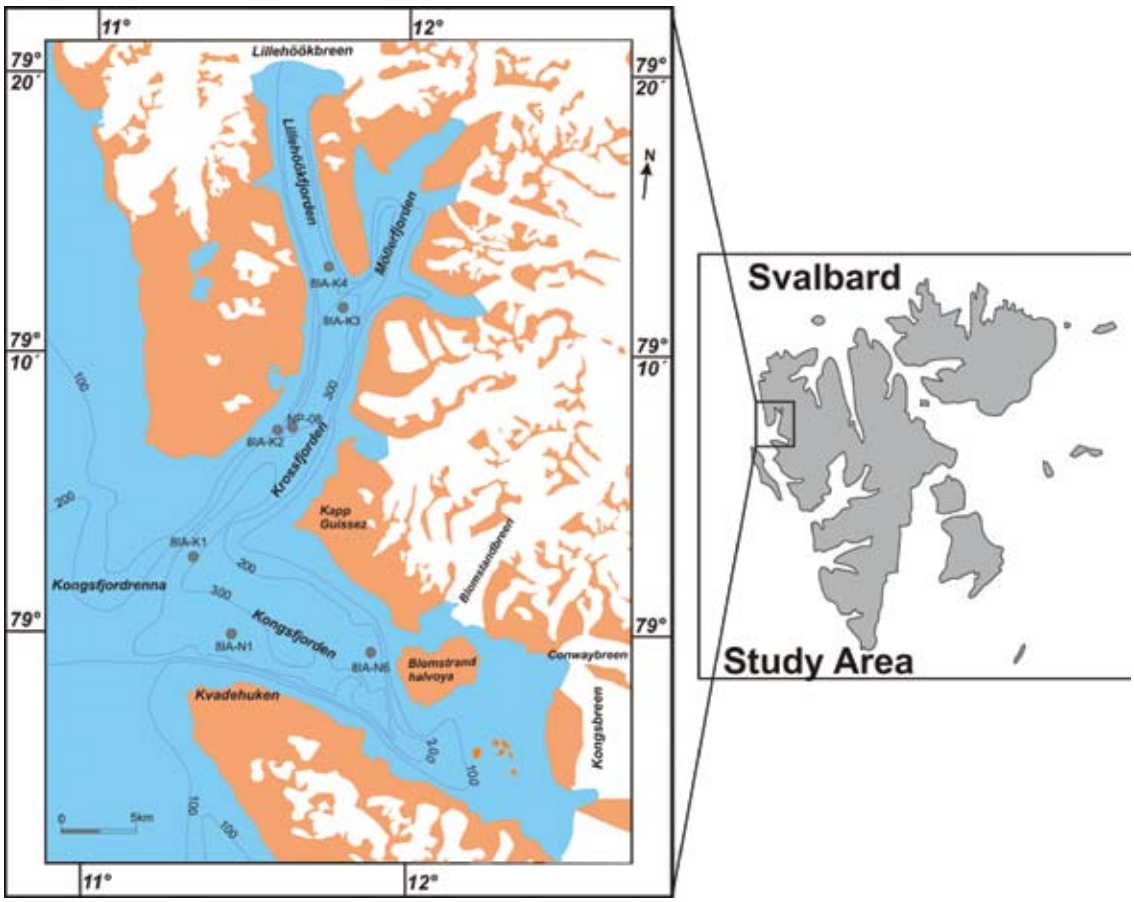

Fig.50.: Map showing the study area (map modified after Svendsen et al. 2002) [3] and sediment sampling sites (gray filled circles) with sample name. White color areas are the ice cover on the land part.

References

[1] Ziaja W (2001), Arct. Antarct. Alp. Res. 33 (1): 36-41
[2] Hagen J O et.al, Polar Research, 22(2): 145-159
[3] Svendsen H et.al (2002), Polar Research 21(1): 133-166